Seed tuber microbiome can predict growth potential of potato varieties

Song, Yang; Atza, Elisa; Sánchez-Gil, Juan J.; Akkermans, Doretta; de Jonge, Ronnie; de Rooij, Peter G.H.; Kakembo, David; Bakker, Peter A.H.M.; Budko, Neil V.; More Authors

DOI
10.1038/s41564-024-01872-x

Publication date
2024

Published in
Nature Microbiology

Citation (APA)
Song, Y., Atza, E., Sánchez-Gil, J. J., Akkermans, D., de Jonge, R., de Rooij, P. G. H., Kakembo, D., Bakker, P. A. H. M., Budko, N. V., & More Authors (2024). Seed tuber microbiome can predict growth potential of potato varieties. *Nature Microbiology*, *10*(1), 28-40. Article 4536. https://doi.org/10.1038/s41564-024-01872-x

nature microbiology

Article

https://doi.org/10.1038/s41564-024-01872-x

Seed tuber microbiome can predict growth potential of potato varieties

Received: 16 April 2024

Accepted: 31 October 2024

Published online: 27 December 2024

Check for updates

Yang Song[1], Elisa Atza[2], Juan J. Sánchez-Gil[1], Doretta Akkermans[3], Ronnie de Jonge[1,4], Peter G. H. de Rooij[1], David Kakembo[1], Peter A. H. M. Bakker[1], Corné M. J. Pieterse[1], Neil V. Budko[2] & Roeland L. Berendsen[1]

Potato vigour, the growth potential of seed potatoes, is a key agronomic trait that varies significantly across production fields due to factors such as genetic background and environmental conditions. Seed tuber microbiomes are thought to influence plant health and crop performance, yet the precise relationships between microbiome composition and potato vigour remain unclear. Here we conducted microbiome sequencing on seed tuber eyes and heel ends from 6 potato varieties grown in 240 fields. By using time-resolved drone imaging of three trial fields in the next season to track crop development, we were able to link microbiome composition with potato vigour. We used microbiome data at varying taxonomic resolutions to build random forest predictive models and found that amplicon sequence variants provided the highest predictive accuracy for potato vigour. The model revealed variety-specific relationships between the seed tuber microbiome and next season's crop vigour in independent trial fields. With a coefficient of determination value of 0.69 for the best-performing variety, the model accurately predicted vigour in seed tubers from fields not previously included in the analysis. Moreover, the model identified key microbial indicators of vigour from which a *Streptomyces*, an *Acinetobacter* and a *Cellvibrio* amplicon sequence variant stood out as the most important contributors to the model's accuracy. This study shows that seed potato vigour can be reliably predicted based on the microbiota associated with seed tuber eyes, potentially guiding future microbiome-informed breeding strategies.

The plant microbiome substantially impacts plant growth and health[1]. Although some microorganisms can cause disease, others can support plant growth by mobilizing soil nutrients and protecting against pests and diseases[2–4]. Plants try to shape the plant microbiome to their advantage[5] and can recruit protective microorganisms in response to pathogen or insect attack[6]. As a result, plants can assemble plant-protective microbiomes that survive in soils to protect subsequent plantings. In contrast, pathogen build-up can result in negative soil feedback, reducing growth in subsequent generations[7]. Plant microbiomes that affect plant performance can thus be inherited, which is especially relevant for crops that are propagated via organs from the soil, such as potato tubers.

Potato, the third most important crop for human consumption, plays a crucial role in feeding the world and yields five times more consumable weight per hectare than rice and wheat, making it crucial for global food security[8,9]. Unlike most other major field crops, potatoes are primarily propagated vegetatively by transplanting seed tubers from one field to another in the next growing season.

Substantial variation in seed potato growth potential, or 'potato vigour', is observed when seed potato tubers of the same variety

A full list of affiliations appears at the end of the paper. e-mail: r.l.berendsen@uu.nl

originate from different fields. Potato vigour refers to the physiological potential for rapid and even outgrowth, good emergence and proper development of new shoots sprouting from the tuber eyes[10]. Eyes are the dormant buds or growth points present on the surface of a potato tuber from which new shoots sprout during the early stages of potato plant growth. Potato vigour is highest at the end of a dormancy phase, after which it declines with ageing of the tubers during storage. Vigour also depends on the genetic background of a potato because both the length of the dormancy period and the subsequent rate of ageing differ between potato cultivars[11]. Potato vigour is also strongly influenced by the growth history of the mother plants that produced the seed tubers[12,13]. When seed tubers of the same variety but from different production fields are planted together in the next season, abiotic and biotic differences in the field of production can lead to varied physiological and microbial imprints in the seed tuber, leading to differences in vigour[14,15]. This variation impacts crop yield and quality yet no reliable diagnostic tool currently exists to assess potato vigour[11].

Studies have shown the significant impact of the potato tuber microbiome on plant health and productivity[16–18]. Although pathogens can be carried by seed tubers[19,20], the tuber can also host beneficial microorganisms that promote plant growth[16,17,21]. Tubers produced in different fields harbour distinct microbiomes that can impact the microbiome of potato roots and even new tubers in a subsequent growing season[14,22,23]. Here we investigated whether the field-specific microbiomes carried by the tuber are associated with potato vigour, as exemplified by the extent of outgrowth of new shoots during early stages of plant growth in the new growing season. We used microbiome amplicon sequencing of a large set of field-collected tubers and extensive time-resolved, drone-based imaging of potato crop development in the next season to build a model that can reliably predict vigour of seed potatoes. Moreover, our model identifies microbial sequences that are potato-variety-specific predictors of potato vigour.

Results

Field of production affects seed tuber vigour

Variability in potato vigour caused by physiological and microbial imprinting of the seed tuber in its field of production is a major issue in the potato production system. To assess this variability, we collected seedlots (batches of seed tubers from individual fields) of 6 different potato varieties, each variety harvested from 30 production fields across the Netherlands in the autumn of 2018 (year 1) and 2019 (year 2; Fig. 1a and Extended Data Fig. 1). In both years, seed tubers from 180 seedlots were stored over winter and planted in 3 trial fields the following spring. In both years, the 3 trial fields were located on farms near Montfrin (M) in France and near Kollumerwaard (K) and Veenklooster (V) in the Netherlands (Extended Data Fig. 1c). In each of the trial fields, the seed tubers were planted in a randomized block design with 4 replicate blocks of 24 tubers evenly distributed over 4 ridges (Fig. 1b,c and Extended Data Fig. 1). We monitored the growth and development of the plants that emerged from these seed tubers using aerial images of the complete field with a drone-mounted camera from 30 days after planting (DAP) until 50 DAP, when leaf canopies of neighbouring plants began to overlap and there were no more empty ridges detected (Supplementary Table 1). As a measure for potato vigour, we corrected for spatial heterogeneity in the field (Extended Data Fig. 2) and quantified the canopy surface area (CSA) of each replicate block (Fig. 1c).

Across both years and all trial fields, we observed that the CSA of the 6 potato varieties developed at substantially different variety-specific growth rates (Fig. 1d and Supplementary Fig. 1) but also with significant variation in the performance of the distinct seedlots within each variety (Fig. 1e–g and Supplementary Fig. 2). We calculated Pearson correlations to assess the relationship between the CSA of different seedlots in each trial field and found a strong overall correlation ($P < 0.001$) for all pairwise comparisons of CSA across trial fields in both experimental years (Fig. 1e–g and Supplementary Table 2), showing that potato vigour of a seedlot in 1 trial field is correlated to the vigour of the same seedlot in another trial field. For the 6 varieties independently, 31 of 36 pairwise comparisons of seedlot CSA were significantly correlated (Supplementary Table 2). Three of the 5 non-significant correlations were probably due to herbicide treatment in field V in year 2, which particularly affected the early-emerging varieties Colomba and Innovator. The majority of the correlations were thus significant, suggesting that the rate of canopy development is an intrinsic property of the seedlot and that potato vigour affects plant outgrowth in the next season. For the variety Festien (Fig. 1h and Supplementary Fig. 2), and other varieties (Extended Data Fig. 3), this seedlot-dependent variation in potato vigour is consistent in all three trial fields, as is visible when CSAs were normalized for the average of the variety in each field (scaled CSA). Seedlots consistently perform above (green in Fig. 1h) or below (red) the variety's average vigour. Together these data suggest that rate of canopy development reflects the potato vigour of a tuber seedlot at the time of planting in the trial field and that part of potato vigour is imprinted during growth of the seed tuber in the production field.

Edaphic factors and plant genotype affect tuber microbiome

To determine whether variation in potato vigour among seedlots is linked to differences in the composition of the tuber microbiome, we sampled tubers in the months following harvest. From the 180 seedlots harvested annually for vigour assessments (Fig. 1), we selected a subset of 60 seedlots from year 1 for microbiome analysis (Supplementary Table 3) and used 4 replicate samples of 50 tubers per seedlot (240 samples in year 1). After preliminary analysis showed high similarity among replicates, we reduced the number to 2 replicates per seedlot in year 2 but analysed all 180 seedlots (360 samples in year 2; Extended Data Fig. 1). From those 600 tuber samples from 240 distinct seedlots across 2 experimental years, we independently sampled tuber eyes and tuber heel ends, and subsequently sequenced 16S rRNA and internal transcribed spacer (ITS) regions of the bacterial and fungal DNA, respectively (Extended Data Fig. 1). After clustering sequencing reads into amplicon sequence variants (ASVs) and filtering out ASVs occurring in less than 2 samples and less than 30 reads, we identified a total of 17,874 bacterial ASVs and 1,755 fungal ASVs in the eye compartments, and 20,119 bacterial ASVs and 1,917 fungal ASVs in the heel-end compartments of tubers (Supplementary Fig. 3 and Supplementary Table 4).

To identify microbiome signatures across soil type, potato variety and harvesting year, we computed the Bray–Curtis dissimilarity for all pairwise sample combinations and performed a principal coordinate analysis (PCoA). A permutational multivariate analysis of variance on the tuber eye data showed significant ($P = 0.001$) effects of soil type, variety and year on the composition of bacterial (Fig. 2a–c) and fungal (Fig. 2d–f) tuber eye microbiomes. Soil type and variety explained 11% and 12%, respectively, of bacterial community variation and the year of harvest explained 2%. This suggests that the tuber eye microbiome is shaped by a combination of edaphic factors and plant genotype. Notably, microbiomes of tuber eyes were similar when samples were derived from the same seedlot and significantly distinct ($P < 0.01$) from those of other seedlots (Extended Data Fig. 4 and Supplementary Fig. 4). This again underlines that the field of production shapes the seed tuber microbiome[14]. Similar results were observed for the heel-end compartment (Extended Data Fig. 5).

Microbiome-based predictions of seed tuber vigour

Having established that seedlots within each variety clearly vary in both vigour and microbiome composition, we explored whether a model could predict seedlot vigour using microbiome fingerprints from seed tuber eyes. Recently, machine-learning techniques have been successfully applied to microbiome data[24–26] and so we constructed a microbiome data-based random forest (RF) model[27] to predict potato vigour. To determine the optimal taxonomic rank for prediction, we

https://doi.org/10.1038/s41564-024-01872-x

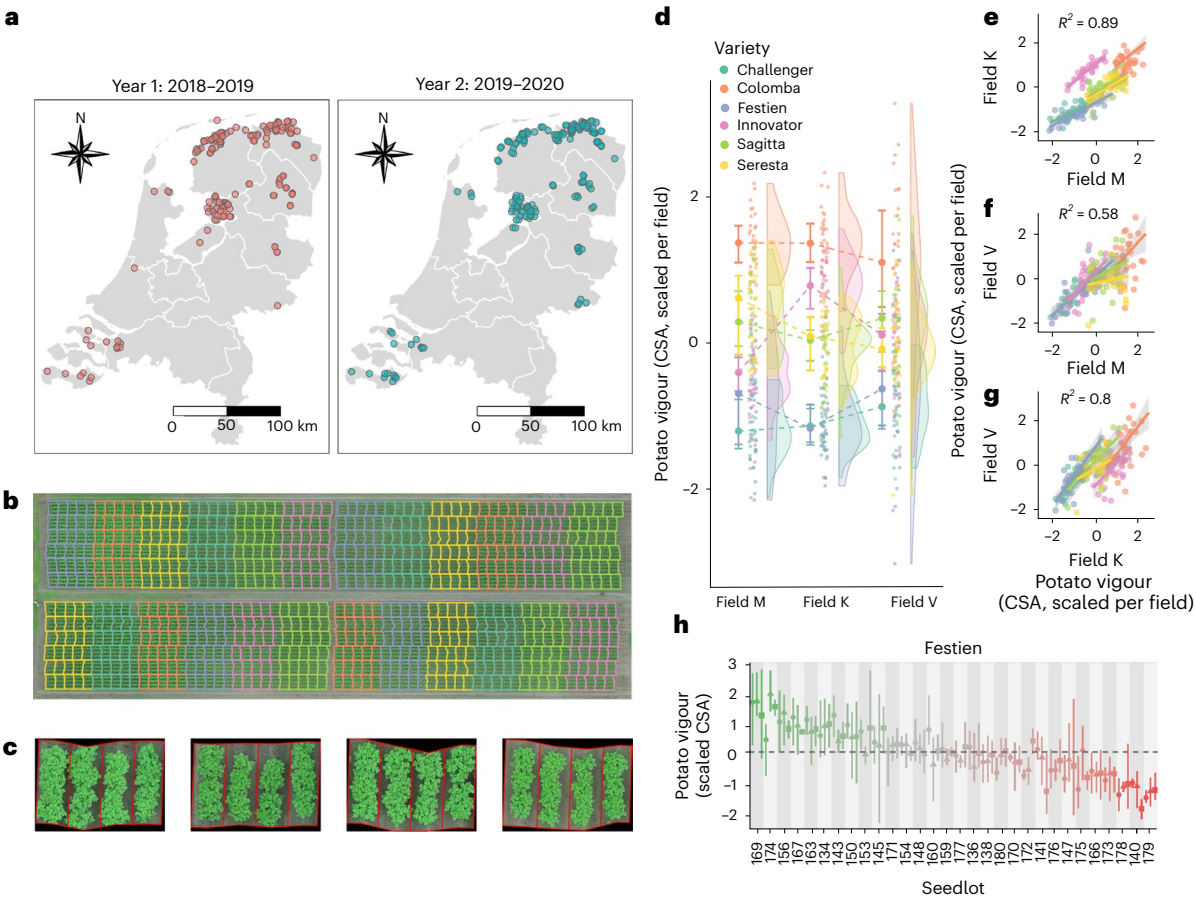

Fig. 1 | Variation in canopy development of potato plants from 6 varieties and 180 production fields. a, Locations of the 180 fields per year where the seedlots of 6 potato varieties (30 fields per variety) were collected in the Netherlands (52.3676° N, 4.9041° E). **b**, Drone image showing the complete randomized block design in trial field V in year 2. All 30 seedlots of the varieties Challenger (teal green), Colomba (salmon), Festien (blue), Innovator (mauve), Sagitta (green) and Seresta (yellow) were planted in 4 replicated blocks. Within a block, tubers of each seedlot were planted in a plot of 4 × 6 tubers. **c**, Exemplary images of four replicate plots of the same seedlot in trial field M. **d**, Potato vigour, represented by CSA (scaled per field), of all 180 seedlots in year 1 in field M, K and V at 52 DAP, 48 DAP and 50 DAP, respectively. Colours denote the different varieties in the study, each variety represented by 30 seedlots in each trial field. For every variety in each field, the dots depict the median CSA for the 30 seedlots and the error bars indicate the 25th and 75th percentile. CSA was scaled by subtracting the mean CSA of all plots in each trial field and dividing it by the CSA standard deviation. **e**–**g**, Correlations of CSA (scaled per field) between trial fields K and M (**e**), between trial fields V and M (**f**) and between trial fields V and K (**g**). R^2 values result from fitting a linear mixed model to CSA using plant varieties as random effects. The Pearson correlations of CSA across fields of all varieties or per variety are depicted in Supplementary Table 2. Error bands around the regression line represent 95% confidence intervals. **h**, Effect of each seedlot on the growth of Festien plants in each of the 3 trial fields in year 1, with green representing seedlots performing above average and red representing seedlots performing below average. Scaled CSA was calculated per trial field by subtracting the mean CSA of the variety and dividing it by the variety's CSA standard deviation. Symbols and error bars show the average, minimum and maximum CSA values of four replicate plots of each seedlot per trial field, after correcting raw CSA values for spatial heterogeneity. Circles indicate trial field M; triangles indicate trial field K and squares indicate trial field V.

assessed model performance using distinct taxonomic levels: ASV, species, genus, family, order and class. Moreover, we used hierarchical feature engineering (HFE)[28] to generate an additional feature level. HFE is a method used for feature engineering in machine learning that incorporates hierarchical information into the feature representation. It leverages the hierarchical structure of microbiome data and selects features of different taxonomic ranks to optimize the prediction.

To avoid predicting differences in CSA resulting only from genetic differences between potato varieties, we used scaled CSA values per trial field and variety (hereafter referred to as CSA) to train our RF model to minimize the error in fitting out-of-bag (OOB) samples. We trained the model on the bacteria data of year 2 and potato vigour data (CSA) in trial field M of the same year (training set). As a control, we tested the model by correlating the predicted CSA to the observed CSA in the same field. As expected, the model very accurately predicted the CSA for the data it was trained on (coefficient of determination (R^2) = 0.98 for ASV-level predictions on field M). The OOB R^2 is a more unbiased estimate of the model's performance. For field M, the OOB R^2 performance was highest when the model was based on the hierarchically engineered features (HFE; R^2 = 0.34), followed by the model based on ASVs (R^2 = 0.22; Fig. 3).

We then tested the model, trained on field M data, for its ability to predict CSA in the other two trial fields from the same year (within-year testing set, fields K and V). The model produced significant correlations between predicted and observed CSA in these fields, regardless of taxonomic rank of the bacterial data (within-year testing set; Fig. 3). For within-year predictions, training the model on HFE resulted in similar R^2 values as when the model was trained on ASV features. Within-year predictions, however, are all based on microbiome data from the same year. We then further tested the RF model using the tuber microbiome data from year 1 (across-year testing set), to which our model was completely naive. Although the prediction performed better for fields within the same experimental year, even the prediction based on the seedlot microbiomes from this preceding year that were not used to

https://doi.org/10.1038/s41564-024-01872-x

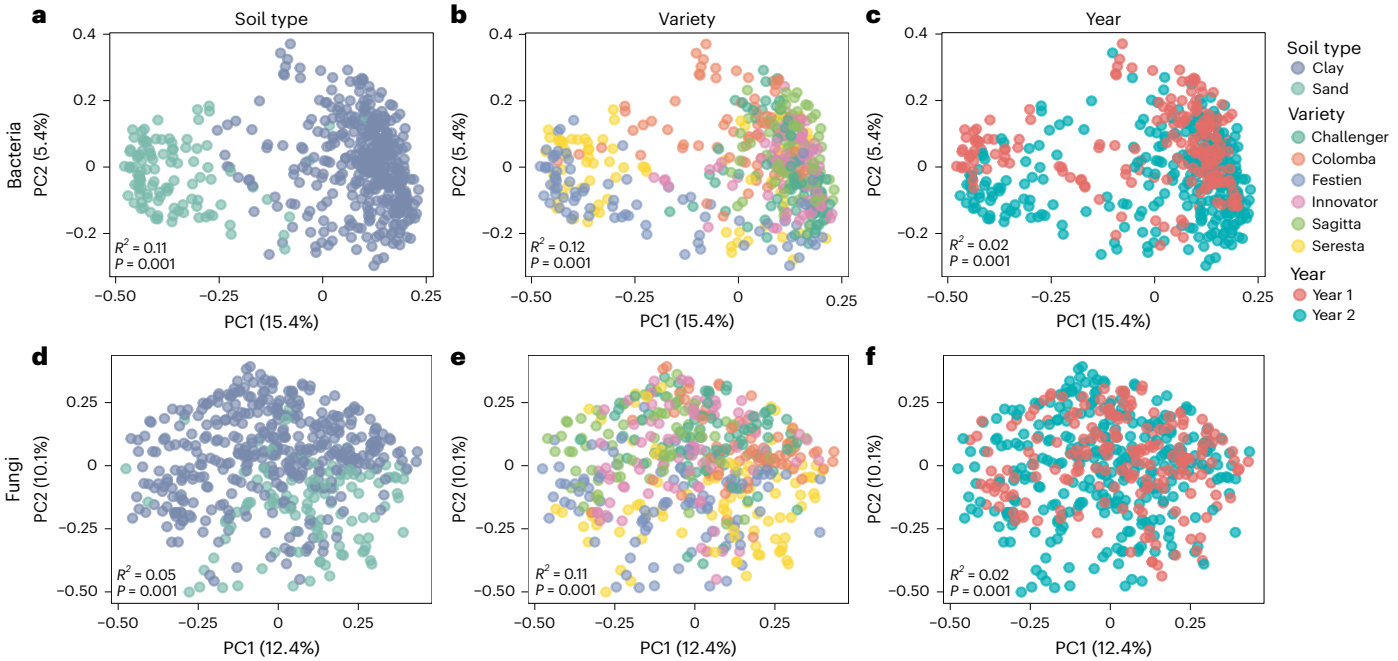

Fig. 2 | Community composition analysis of seed tuber microbiomes in the tuber eye compartment. a–f, Principle coordinate analysis (PCoA) ordination plot based on Bray–Curtis dissimilarities of bacterial microbiomes coloured by soil type (**a**), variety (**b**) and year (**c**), and fungal microbiomes coloured by soil type (**d**), variety (**e**) and year (**f**), as indicated in the legend. Each data point represents a single replicate of a seedlot. Four replicate samples were analysed for each of the 60 seedlots in year 1 and 2 replicate samples were analysed for each of the 180 seedlots in year 2. *P* (one sided) and R^2 values in each principal component analysis are the result of permutational multivariate analysis of variance on soil type (**a**,**d**), variety (**b**,**e**) and year (**c**,**f**) factors.

train the RF model were significantly correlated to the observed vigour of the seedlots. Here, the HFE-based RF model (maximum $R^2 = 0.1$; Fig. 3, bacteria) was outperformed by the RF model trained at the ASV level (maximum $R^2 = 0.18$).

Subsequently, we compared the performance of RF models that were built on either bacterial data alone, fungal data alone, or combined bacterial and fungal data (Fig. 3). Training on fungal data alone resulted in reasonably similar model performance with the within-year data but led to lower model performance on the across-year testing set compared with the model based only on bacteria at any phylogenetic level (Fig. 3). Combining bacterial and fungal ASV tables slightly improved the predictions of the bacteria-only RF model for both the within-year and across-year testing sets (Fig. 3).

Collectively, our results show that our 'potato-microbiome informed' (PMI) predictive model based on microbiome fingerprints of seed tubers can predict potato vigour in the next growing season. The PMI model performs most accurately across year when using the highest taxonomic resolution at the ASV level and improves when both bacterial and fungal data are included. We also trained RF models on heel-end microbiome data (Supplementary Table 5), which performed slightly less accurately than those based on tuber eye microbiomes. Therefore, we focused on tuber eye microbiomes (henceforth tuber microbiome) for the rest of the study.

Real-world application of the PMI model

For potato producers, seed tubers represent a large annual investment and, hence, their vigour is of considerable importance. The PMI model's predicted potato vigour (CSA values) significantly correlated with observed CSA values for both within-year and across-year testing sets (Spearman correlation; Fig. 4).

To intuitively evaluate the performance of the PMI prediction model, we divided the seedlots into 3 classes based on their predicted and observed vigour (CSA value): high vigour (H; 1/3 of the seedlots with highest vigour), low vigour (L; 1/3 of the seedlots with lowest vigour) and medium vigour (M; remaining 1/3 of the seedlots). We then calculated the precision value of the model (confusion matrix in Fig. 4), which represents the percentage of correctly predicted samples within each respective class. Whereas the model predicts L or H classes relatively accurately, the model appears to have more difficulty distinguishing M from L or H, especially in the across-year testing set (confusion matrix, Fig. 4b). As users will be most interested in knowing the chance that a seedlot that is predicted to have high vigour is not in reality a seedlot with observed low vigour, or the other way around, we introduced a 'quality confidence' metric, which assesses the likelihood that a seedlot predicted as H or L is correctly classified and not the opposite (quality confidence in Fig. 4). In the within-year testing set, this yielded a high quality confidence score of 85–100% of the seedlots that were predicted to be H or L in reality not being the opposite (L or H). Notably, even in the across-year testing set, only a small percentage (5–22%) of seedlots were misclassified and predicted in the opposite class. For instance, of the seedlots that were predicted to have high vigour, 90–93% had a high or medium observed vigour and only 7–11% were misclassified as low vigour. Conversely, of the seedlots that were predicted to have low vigour, 78–82% indeed had an observed low or medium vigour and only 18–22% were misclassified as high vigour, which is significantly lower than random ($P < 0.001$; Fig. 4b). Despite lower precision in across-year prediction (confusion matrix, Fig. 4b) than within-year prediction (confusion matrix, Fig. 4a), the quality confidences indicate that the model still showed favourable performance in predicting the H or L class. This shows that the prediction model is fairly accurate in predicting potato vigour extremes and that the model has real-world applicational value in assessing potato vigour.

Performance of the model differs across potato varieties

The model described above was designed as a variety-generic model trained on data from all 6 potato varieties used in this study. When looking into each individual variety, within the same year, the potato

https://doi.org/10.1038/s41564-024-01872-x

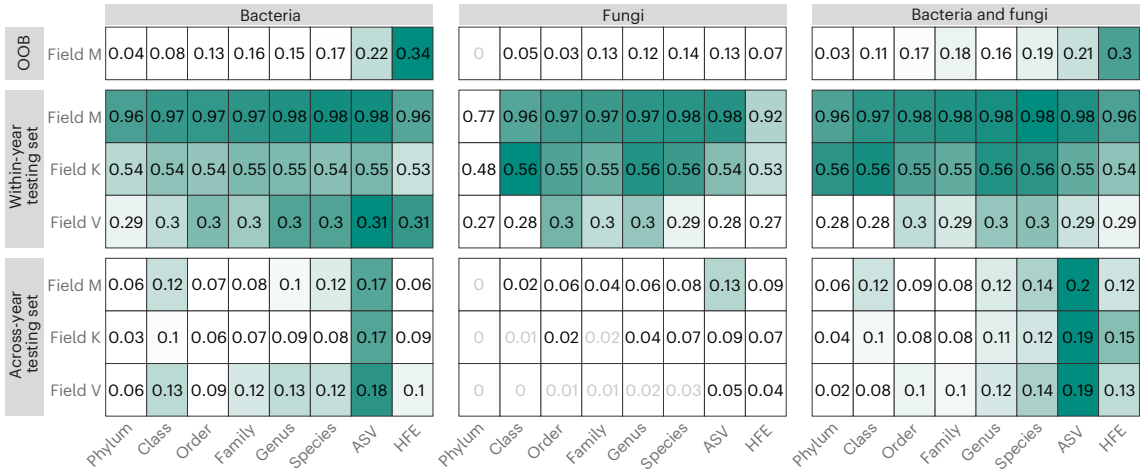

Fig. 3 | Performance of RF models trained with tuber eye microbiome data at distinct taxonomic ranks and HFE features. RF models trained on tuber microbiome data and field M potato vigour in year 2 were tested on vigour data from field M (training set); field K and V in year 2 (within-year testing set); and then tested on data from field M, K and V in year 1 (across-year testing set). RF models were trained on 16S data (Bacteria), ITS data (Fungi) or both data sets combined (Bacteria and fungi). Numbers represent the R^2 of a model, where a higher value indicates superior performance. The cell colour intensity corresponds to the R^2 value, with higher values represented by more intense colours. The intensity scale is normalized independently for each row to emphasize relative performance within that row. OOB indicates the OOB performance of the models in the training set.

vigour CSA values predicted by the model correlate significantly with the observed CSA values for each of the 6 varieties. Although the quality confidence for each of the varieties varies, it is generally high (82–100%) within years (Fig. 5a).

However, across-year predictions revealed bigger differences in model performance across potato varieties. Spearman correlation analysis indicated a significant positive correlation between predicted and observed vigour for the varieties Challenger, Festien and Innovator, which indicated that the model showed stronger predictive performance for these varieties (Fig. 5b and Extended Data Fig. 6). The across-year prediction was less informative for the varieties Colomba, Sagitta and Seresta. This shows that the PMI model does not work equally well for all varieties. Nonetheless, although the correlations between observed and predicted potato vigour values are not significant for Colomba, Sagitta and Seresta, the quality confidence parameter still provides relatively high scores (86–90%) for the high-vigour seedlots classified as H (Fig. 5b).

Key microbial predictors of potato vigour

The PMI model's predictions are based on the occurrence and abundance of 19,629 bacterial and fungal ASVs detected on potato tuber eyes across the Netherlands. To identify microbial taxa that are key predictors of potato vigour, we ranked ASVs by their contribution to the model's accuracy. The top ASVs that together accounted for 1% (20 bacterial and 2 fungal ASVs) or 5% (96 bacterial and 14 fungal ASVs) of the model's accuracy were selected (Fig. 6a). Most key ASVs corresponded to Pseudomonadota, Actinomycetota or Bacteroidota (Fig. 6b). These ASVs showed consistent prevalence and abundance across both experimental years (Supplementary Fig. 5) and showed both positive and negative correlations with tuber vigour (Fig. 6c–e and Extended Data Figs. 7 and 8). The three ASVs that contribute the most to the prediction of the PMI model are *Streptomyces* ASV 6c8e8, *Acinetobacter* ASV bcae8 and *Cellvibrio* ASV c205d. Here, we used the first five characters of the automatically generated ASV identifiers to designate individual ASVs. Whereas the abundance of *Streptomyces* ASV 6c8e8 on the tuber is positively correlated with tuber vigour, higher abundances of *Acinetobacter* ASV bcae8 and *Cellvibrio* ASV c205d are negatively correlated with potato vigour (Fig. 6c,d).

One advantage of the RF algorithm is that the reported important ASVs do not necessarily correlate linearly with potato vigour CSA values. Instead, the PMI model can capture more complex relationships that can be examined with partial contributions. The partial contribution of an ASV represents how the predictions of potato vigour change according to the counts of that individual ASV. To explore the relationship of each of the top 1% ASVs with potato vigour, we computed the partial contributions of each ASV to the model predictions (Extended Data Fig. 7b). *Streptomyces* ASV 6c8e8 was the best predictor of vigour. The vigour of the tubers in which this particular ASV was not detected was below average; however, on the tubers that did have this ASV, increased abundance of ASV 6c8e8 was associated with improved potato vigour. In addition, although this *Streptomyces* ASV is both prevalent and abundant in most microbiome samples (Fig. 6f,g), Fig. 6d shows that above a threshold level of approximately 30 counts per sample, potato vigour is not further improved. This suggests that the absence of *Streptomyces* ASV 6c8e8 on the seed tuber in particular is a crucial indicator of low potato vigour. In contrast, the presence of *Acinetobacter* ASV bcae8 and *Cellvibrio* ASV c205d are indicators of relatively low potato vigour. Moreover, reduced vigour of the tubers correlated with increased abundance of these ASVs. Notably, the negative correlation between abundance of these ASVs and vigour of the tubers appears to reach a plateau, after which further increase in abundance of these microorganisms has no additional negative effect on potato vigour (Fig. 6d).

Although key predictive microorganisms were identified from data across all varieties, their correlation with vigour was not always consistent across individual varieties (Fig. 6e and Extended Data Fig. 8). This suggests that different varieties are linked to specific key microorganisms. Together, these results show that identifying key microorganisms predictive of seed tuber vigour is feasible and that these microorganisms could be developed as biomarkers for potato vigour.

Discussion

The vigour of potato seed tubers, as indicated by canopy development of the emerging shoots, varies[14,29]. Seed tubers harbour a microbiome that is largely assembled in the production field and carried into the planting field[14]. Microorganisms on a seed tuber probably partly reflect the physiological state of that tuber, but tuber-borne microorganisms can also affect the growth of the plant that emerges from a tuber[30,31]. Here we show that potato tuber vigour can be predicted using tuber microbiome fingerprint data.

https://doi.org/10.1038/s41564-024-01872-x

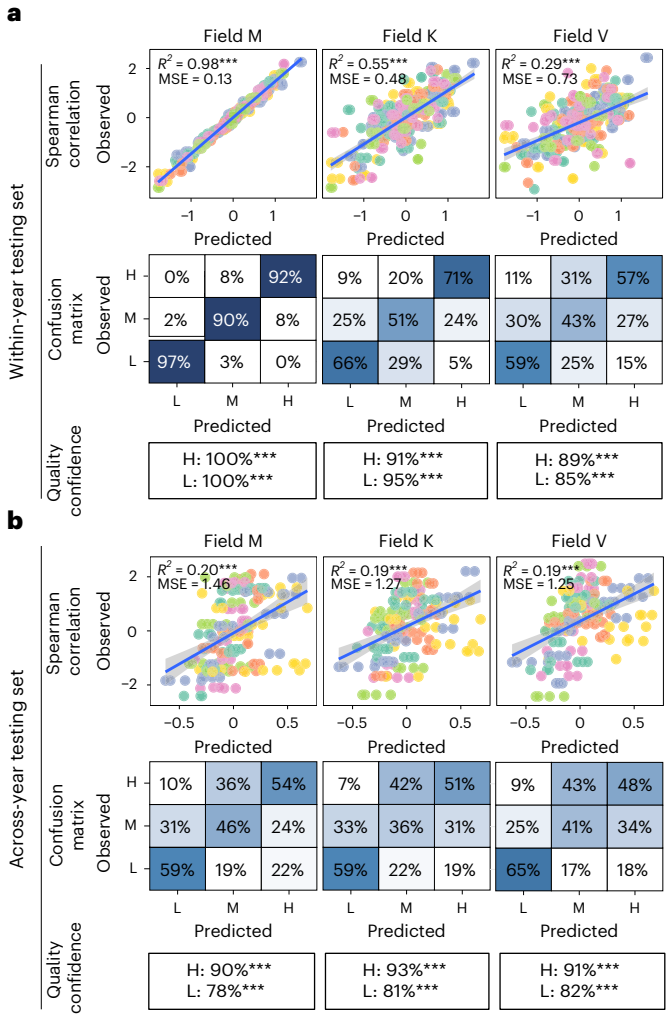

Fig. 4 | Model performance on within-year and across-year test sets over all varieties. a,**b**, Model performance of all varieties and per variety on within-year testing sets (**a**) and across-year testing sets (**b**). Scatter plots show the Spearman correlation between the predicted potato vigour (*x* axis) and observed potato vigour (*y* axis). The colours of dots in the scatter plot indicate the varieties Challenger (teal green), Colomba (salmon), Festien (blue), Innovator (mauve), Sagitta (green) and Seresta (yellow). The predicted values are generated by the PMI model trained on microbiome data from year 2 and CSA from field M of year 2. Predicted CSA is either based on the same microbiome data (within year) or on microbiome data from year 1 to which the model was naive (across year). Predicted and observed CSA is scaled to the variety average in each trial field. Proportion of variance explained by the model is indicated by R^2, and the average squared difference between the observed and predicted CSA is indicated by mean squared error (MSE). Error bands around the regression line represent the 95% confidence interval. The confusion matrices show the precision of the model in identifying H, M and L classes. Intensity of blue shading in the confusion matrices increases with the precision of the model. Also shown is the quality confidence of within-year and across-year predictions, that is, the chance of the H or L class not being misclassified as the opposite extreme class. The asterisks indicate pseudo-*P* values (one sided) of quality confidence being higher than random guess by simulating 1,000 random classifications: ***$P < 0.001$.

Vigour is imprinted in the field of production

After planting, seed tubers develop shoots from their eyes, which grow into a canopy. Our data show that distinct potato varieties show varying rates of canopy development, highlighting the evident relationship between potato genetics and growth. In addition, climatic conditions and soil characteristics in the planting field also influence the rate at which a potato variety develops, resulting in varying average CSAs for each variety in different trial fields. Importantly, even seed tubers of the same variety and grown in the same trial field develop canopies of different sizes, depending on the production field from which these seed tubers originated. We showed that the CSA produced by a seedlot is correlated across trial fields and that seedlots outperforming or underperforming the average of its potato variety, consistently do so across different trial fields. These seed tubers thus show distinct potential for developing CSA, and we considered CSA to reflect the tuber's vigour at the time of planting. As all seedlots in our study were stored under the same conditions in one location, our data underscore that potato vigour is, in part, imprinted in the seed potato tubers by local conditions in their production field. Vegetative growth parameters, such as CSA, have been shown to be good predictors of final potato yield[32–35]. Hence, it is tempting to speculate that the PMI model may also have potential for predicting next-season yield.

Each field produces a unique seed tuber microbiome

We analysed the microbiomes of 240 seedlots across the Netherlands and, consistent with previous studies[14,36,37], found that soil type, harvest year and potato variety significantly affected the microbial signatures of seed tubers. It is well established that abiotic factors, including both edaphic and climatic conditions, influence the soil microbiome[38]. In addition, each field has a distinct pre-crop history, during which each crop species or even variety selectively assembles a distinct microbiome[39]. Agricultural practices also play a role in shaping the microbiome composition of soil[40]. In this way, diverse and unique collections of microorganisms assemble in each soil, from which a distinct selection of microorganisms will colonize the plants. Consequently, we found that seed tubers harbour a distinct microbial fingerprint, depending on the soil in which they were produced.

Microbiome-informed prediction of crop vigour

We were able to link the composition of seed tuber microbiome to plant performance in the subsequent growing season. Using amplicon sequence data of tuber microbiomes from one year, we generated an RF-based PMI potato vigour prediction model that successfully predicted potato tuber vigour in a different year. This shows that the tuber microbiome can predict the outgrowth of emergent plants in the next season, making the PMI model a potentially valuable diagnostic tool for assessing tuber seedlot quality. In addition, the PMI model shows that machine learning has the potential to generate models for vigour assessment of seeds or seedlings of other plant species. In this regard, initial steps have been taken to identify soil microbiome indicators associated with maize growth responses to inoculation of arbuscular mycorrhizal fungi[41]. Also, the occurrence of *Fusarium* disease could be predicted based on soil microbiome composition[26].

Key microbial predictors as causes or consequences of vigour

The PMI model not only predicts the vigour of seed tubers but also ranks the features contributing to the prediction. The key features identified by the model could be considered as biomarkers for vigour. It remains unclear whether these ASVs merely reflect the physiological state of the tubers or actively influence vigour. Nonetheless, there are some indications in the literature that suggest at least some of the key microorganisms play a causal role. The presence of *Acinetobacter* ASV bcae8 is linked to decreased vigour of tubers by our model, which is consistent with observations that *Acinetobacter* sp. strongly reduces the growth of potato seedlings[42]. Moreover, the feature contributing the most to the prediction of our model is *Streptomyces* ASVs 6c8e8, the presence of which appears to be a prerequisite for good vigour. In that respect, it is remarkable that the natural build-up of high densities of pathogen-antagonistic *Streptomyces* spp. in soils is thought to play a key role in natural suppression of potato disease[43–46]. Therefore, our model is also a potential treasure trove for the discovery of unrecognized deleterious or beneficial microorganisms specific to

https://doi.org/10.1038/s41564-024-01872-x

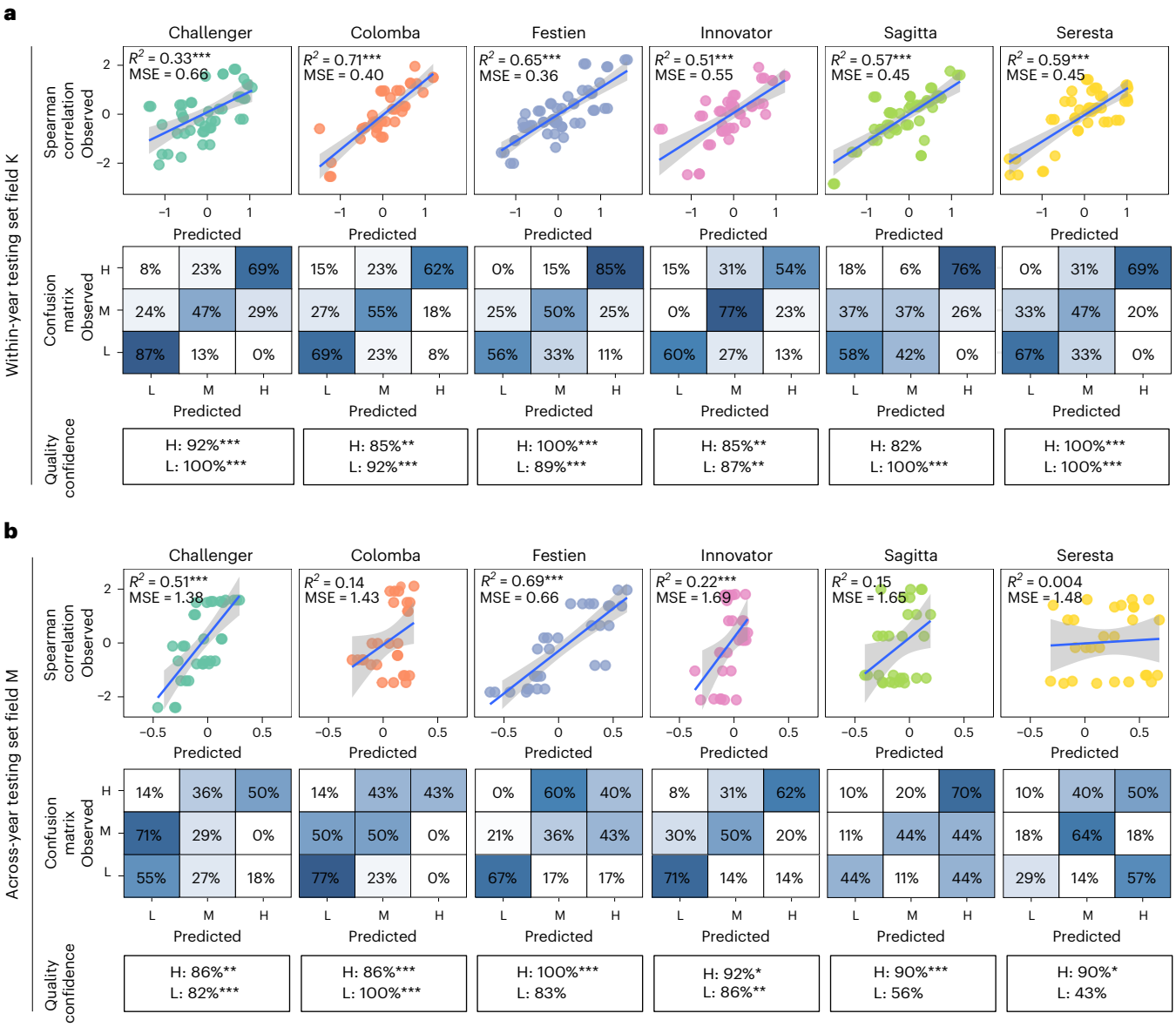

Fig. 5 | Model performance per variety on within-year and across-year test sets. **a**, Model performance per variety on within-year test sets. **b**, Model performance per variety on across-year test sets. Scatter plots show the Spearman correlation between the predicted potato vigour (*x* axis) and observed potato vigour (*y* axis). Predicted values are generated by an RF model trained on microbiome data from year 2 and CSA from field M of year 2. The predicted CSA is either based on the same microbiome data (within year) or on microbiome data from year 1 to which the model was naive (across year). CSA is observed in field K in year 2 (**a**; within year), or in field M, year 1 (**b**; across year). Predicted and observed CSA is scaled to the variety average in each trial field. The proportion of variance explained by the model is indicated by R^2 and the average squared difference between the observed and predicted CSA is indicated by the MSE. Error bands around the regression line represent the 95% confidence interval. The confusion matrices show the precision of the model in identifying H, M and L classes. Also shown is the quality confidence of within-year and across-year predictions, that is, the chance of the H or L class not being misclassified as the opposite extreme class. The asterisks indicate pseudo-*P* values (one sided) of quality confidence being higher than random guess by simulating 1,000 random classifications: $^*P < 0.05$, $^{**}P < 0.01$, $^{***}P < 0.001$.

potatoes. Our current efforts are focused on isolating and identifying the microorganisms that represent the keystone ASVs from potatoes and validating their effects on potato vigour.

A working model and avenues for improvement

Although the current model explains up to 20% of variation in potato vigour, its ability to accurately predict extremes of vigour and reduce misclassification offers significant benefits to potato growers. Improvements could be made by incorporating more data or additional variables, such as soil properties, field planting history or metabolomic properties of the tubers. Using alternative machine-learning algorithms, such as gradient boosting[47] and neural networks[48], could also enhance prediction accuracy. In this study, RF[27] was chosen due to its inherent advantages in handling high-dimensional data, which is characteristic of microbiomes. RF has been widely used in microbiome–host trait predictions in clinical studies, where it often outperforms other models[37,49]. Similarly, in environmental studies, it has shown superior performance in predicting soil disease occurrences based on soil microbiomes[26]. We also opted for an RF regression approach to derive a relative vigour score and to empower users to accurately pinpoint seedlots with high or low vigour, which is more adaptable for practical applications. Finally, we used HFE in this study[28] for feature selection and RF default hyperparameters to train the models. Other methods for feature selection (for example, Fizzy[50] and MetAML[49])

https://doi.org/10.1038/s41564-024-01872-x

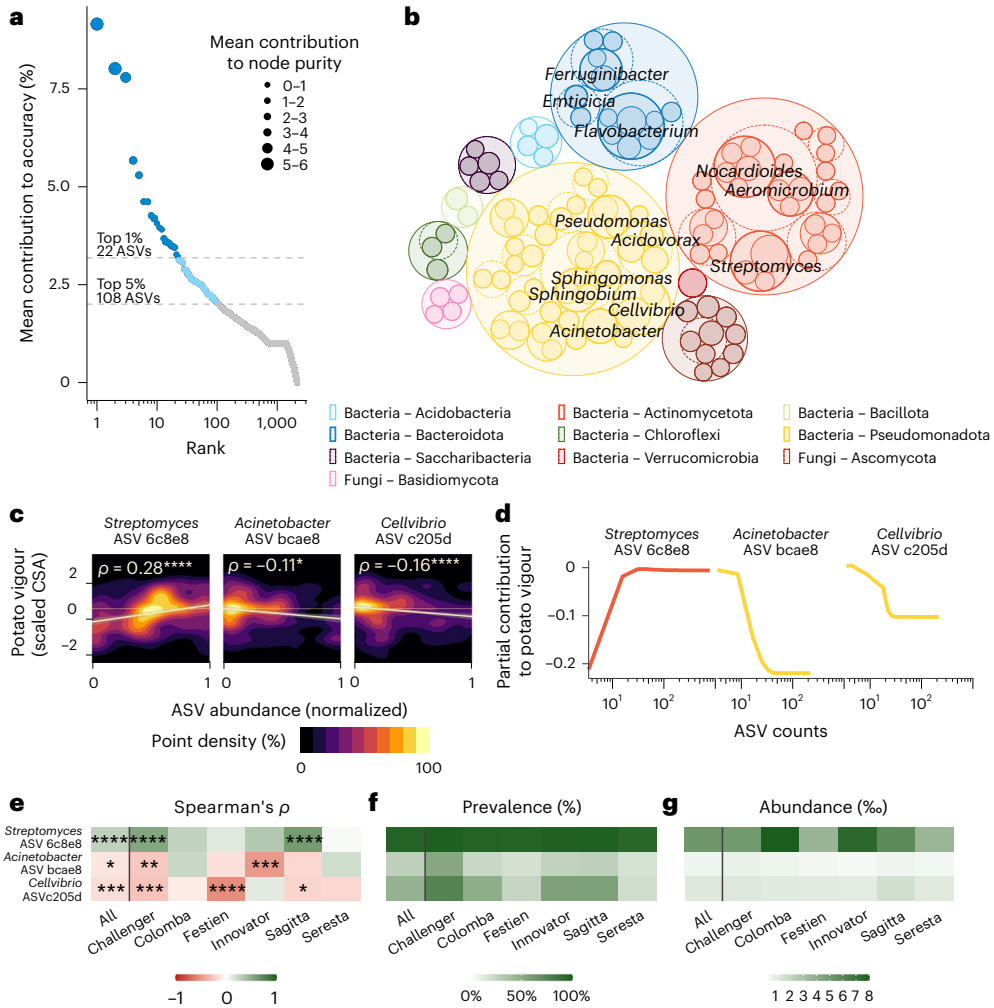

Fig. 6 | The most predictive microorganisms selected by the PMI prediction model. a, Mean contribution to accuracy of the PMI model of each of the ASVs, ranked from highest to lowest contribution. The top-contributing ASVs are highlighted, representing 1% (dark blue colour, 22 ASVs) and 5% (light blue colour, 86 additional ASVs) contribution to the accuracy of our model. The contribution to accuracy is measured as the percent increase in mean squared error of the PMI model. **b**, Bubble plot depicting the phylogenetic composition of the top 5% most-predictive microorganisms, grouped and coloured according to their phylum. The top 1% most-predictive ASVs are highlighted with their genus classification when present. Bubble size indicates the mean contribution to accuracy. **c**, Spearman correlation between the relative abundance of each of the top-3-contributing ASVs and potato vigour. ASV abundance is rescaled between 0 and 1 with respect to its minimum and maximum to show 1 single scale across ASVs. Only non-zero ASV values are used in the plot. The colour represents the density of the sample points. The brightest colours indicate areas that accumulate most of the samples, and dark colours indicate the areas in which no data or few sample points are found. The line represents robust regression to outliers and Spearman's ρ is shown. The asterisks indicate significance level: *$P < 0.05$, **$P < 0.01$, ***$P < 0.001$, ****$P < 0.0001$, two sided, not adjusted for multiple comparison. **d**, Partial contribution plots for the top 3 ASVs most predictive to potato vigour according to the PMI model. **e**–**g**, Heat maps showing Spearman correlations of the top-3-contributing ASVs to potato vigour (**e**), the prevalence of these ASVs (**f**) and their median abundance (**g**) across samples. The first column in each heat map shows the computed value including all the data regardless of plant variety, and the remaining columns show those values calculated for individual potato varieties. In **e**, asterisks indicate significance level of Spearman's ρ: *$P < 0.05$, **$P < 0.01$, ***$P < 0.001$, ****$P < 0.0001$, two sided, not adjusted for multiple comparison.

and hyperparameter tuning are promising avenues to improve the performance of the PMI model[51]. Further refinement of the model with the above-mentioned options should further enhance the model's predictive power and practical utility.

Towards microbiome-optimized potato

We found that the vigour of different potato varieties is linked to specific subsets of microorganisms. This finding aligns with studies showing that plant varieties have divergent sensitivities to both pathogens[52] and beneficial microorganisms[53]. Our data, along with similar approaches linking microbiome composition to plant phenotypes, could be used to unearth interactions of beneficial and deleterious microorganisms with specific genotypes or genetic regions in potato and other crops. This represents a key step towards breeding or engineering crop varieties that are more productive, while requiring fewer inputs by consistently assembling better-functioning microbiomes. This transformative insight not only advances our understanding of microbial contributions to plant performance but also lays the groundwork for a microbiome-based breeding strategy aimed at enhancing the quality of planting material.

Methods

Potato varieties and seedlots

In total, 6 potato varieties form the Royal HZPC Group and Averis Seeds were used in this study, namely, the varieties Challenger, Colomba, Festien, Innovator, Sagitta and Seresta. In the autumn of 2018 (year 1) and 2019 (year 2), we collected batches of seed tubers (seedlots) of 6 potato varieties from 30 different fields per variety (180 fields in total)

in the Netherlands (Fig. 1a and Extended Data Fig. 1). The 360 seedlots (180 in year 1 and 180 in year 2) were shipped to a central location where they were subsequently stored in the dark at 4 °C.

Field trial set-up and vigour measurement

Tuber seedlots from 180 fields per year were stored over winter, after which they were planted in each of 3 trial fields in the following spring. In both years, the trial fields were located near Montfrin (M; 54.4980° N, 5.1090° E) in France and near Kollumerwaard (K; 70.4325° N, 6.9825° E) and Veenklooster (V; 70.3935° N, 6.7080° E) in the north of the Netherlands, respectively. In each of the trial fields, the seed tubers were planted in a randomized block design with 4 replicate blocks of 24 tubers evenly distributed over 4 ridges (Fig. 1b,c and Extended Data Fig. 1). We monitored the growth and development of the plants that emerged from these seed tubers using aerial images of the complete field with a drone-mounted camera. These images were acquired starting from approximately 30 DAP of the seed tubers and continued until around 50 DAP when no more empty ridges were detected (Supplementary Table 1).

RGB image post-processing and canopy measurement

Due to the relatively large scale of the trials and the chosen planting technique, the trial fields did not show the usual regular structure with easily identifiable rows and columns of plots. Therefore, an in-house standardized procedure was developed with minimal manual interaction to detect and identify plots in the trial fields' images. The plot-detection algorithm is defined by six main steps. Step 1: from the provided row–column plot scheme, the expected number N of plots along the ridges of the trial fields is identified. Step 2: the field image in which the canopy size allows for detecting the gaps between the plots along the ridges is selected from the available images of the trial field. Such an image is usually found towards the end of the canopy growth season, where canopies inside a plot are touching but have not yet grown as to bridge the gaps to neighbouring plots. Step 3: the beginning and the end of the trial field along each ridge is interactively determined in the selected image. Step 4: the expected number of $N-1$ interplot gaps are automatically detected in the images along each ridge. Step 5: the detected plot polygons are displayed and inspected for possible remaining inaccuracies and distortions and the wrongly identified plot boundary points are corrected interactively. Step 6: for each plot, a set of image coordinates of the plot polygonal boundary is saved.

To measure the canopy area within the polygonal plot boundary, the image pixels are segmented into two disjoint sets: pixels of the canopy and pixels of the surrounding soil. Then, the canopy pixels are counted and the result is converted to cm^2. This dataset featured a variety of illumination and moisture conditions, both of which affect the colour of pixels. Also, leaf canopy colours have systematic differences between varieties, ranging from light green to almost purple. Therefore, each orthophoto had to be processed individually, resulting in different segmentation filters with date- and field-specific parameters (see ref. 55 for details). In all cases, the quality of segmentation was confirmed by visual inspection of randomly selected plots of each genotype.

After segmentation, the mean canopy area S_{px} (in pixels) over each ridge of each plot was determined by summing all white pixels within the geometrical boundaries of the ridge and dividing by six—the number of plants in each ridge. A canopy area in pixels is converted to its area in cm^2, using the distance d_{cm} between the ridges in the field as was determined by the planting device and recorded as $d_{cm} = 75$ cm in the V and Kollumerwaard-SPNA (K) fields, and $d_{cm} = 74$ cm in the M field. To find the pixel–cm conversion factor, we compute the average pixel distance d_{px} between the adjacent ridges in the field for a specific date (see protocol in ref. 55). Then, the area S_1 of a single pixel in cm^2 is given by:

$$S_1 = \left(\frac{d_{cm}}{d_{px}}\right)^2. \quad (1)$$

Thus, the canopy area S in cm^2 is obtained from the canopy area S_{px} in pixels as:

$$S = S_1 S_{px}. \quad (2)$$

The ridge-mean plot canopies obtained after the transformation, plot localization and segmentation procedures described above constitute the raw data and cannot be used to estimate the mean batch canopy because the test fields are usually spatially inhomogeneous, which may systematically increase or decrease the canopy size in certain areas of the field. We used the state-of-the-art spatial effect removal method implemented in the R package SpATS[54], which removes both random and fixed spatial effects and provides the best linear unbiased estimate of the mean batch canopy size. We apply spatial effect removal to the raw canopy data obtained from all available orthophotos. Raw and spatial-corrected vigour data generated in this project and step-by-step protocol can be found at: https://data.4tu.nl/datasets/21892a06-078a-4600-8386-1abe46f42271 (ref. 55).

Choice of the time point for potato vigour measurement

Our observations indicate that between 47 DAP and 50 DAP (Supplementary Table 1), all plants have emerged and their canopies have not yet begun to overlap. During this crucial period, the final selection of dates for vigour measurements was made. In 2019, the last measuring dates were chosen: 52 DAP for field M, 48 DAP for field K and 50 DAP for field V. In 2020, the second-last measuring dates were chosen: 47 DAP for field M, 47 DAP for field K and 49 DAP for field V. It is important to note that these specific date choices do not significantly impact the subsequent prediction modelling or alter the conclusions drawn from the analysis because the data from the last two to three time points are highly correlated (Supplementary Table 2). To remove the apparent strong genotype effect, we scaled the CSA data for each genotype within each trial field. This means that from each CSA measurement we subtract the average CSA of the variety in the trial field and divide it by the variety's standard deviation.

Sampling of seed tubers for microbiome analysis

In both years, seed tubers were harvested between September and October and stored at 4 °C until they were sampled in December or January. Cores (1 cm thick) were sampled from potato heel ends or eyes using a sterilized metal corer with a diameter of 0.6 cm. Cores from 50 seed tubers were pooled into a single sample per compartment per seedlot for each biological replicate. For each of the 6 varieties, we sampled 4 replicates for each of 10 seedlots in year 1 (240 samples per compartment) and 2 replicates of 30 seedlots in year 2 (360 samples per compartment). In total, 30,000 tubers (12,000 in year 1 and 18,000 in year 2) were sampled to access the microbial composition of different tuber compartments, resulting in 600 samples per compartment. These samples were snap-frozen in liquid N_2, freeze-dried and stored in 50 ml Falcon tubes at −20 °C until further processing.

Sample grinding

To efficiently grind the samples in a high-throughput manner, the freeze-dried samples in 50 ml Falcon tubes were amended with 4 sterile metal beads (5 mm) per tube and placed in a custom-made wooden adaptor in a paint shaker machine (SK550 1.1 heavy-duty paint shaker; Fast & Fluid) followed by vigorous shaking for 9 min on maximum intensity (indication of rpm). Freeze-dried sprout samples in 2 ml Eppendorf tubes were ground with 1 sterile metal bead (5 mm) per tube with a TissueLyser II (Qiagen) at 30 Hz for 1 min.

DNA isolation, library preparation and sequencing

Genomic DNA was isolated from ±75 mg eye or heel-end powder per sample using a Qiagen PowerSoil KF kit (Qiagen). The KingFisher Flex Purification System machine was used for high-throughput DNA

isolation. DNA was quantified using a Qubit Flex Fluorometer with the Qubit dsDNA BR Assay Kit (Invitrogen) and normalized to a concentration of 5 ng μl^{-1}. The resulting DNA samples were then stored at −20 °C.

Bacterial 16S rRNA genes within the V3–V4 hypervariable regions were amplified using 2.5 µl DNA template, 12.5 µl KAPA HiFi HotStart ReadyMix (Roche Sequencing Solutions), 2 µM primers B341F (5′-TCGTCGGCAGCGTCAGATGTGTATAAGAGACAGCCTACGGGNGGCWGCAG-3′) and B806R (5′-GTCTCGTGGGCTCGGAGATGTGTATAAGAGACAGGACTACHVGGGTATCTAATCC-3′)[43] with Illumina adaptor sequences in combination with 2.5 µM blocking primers mPNA (5′-GGCAAGTGTTCTTCGGA-3′) and pPNA (5′-GGCTCAACCCTGGACAG-3′) in 25 µl reactions. Blocking primers were used to avoid the amplification of mitochondrial (mPNA) or plastidial (pPNA) RNA from the plant host[44]. Cycling conditions for 16S rRNA were (1) 95 °C for 3 min; (2) 95 °C for 30 s, 75 °C for 10 s, 55 °C for 30 s and 72 °C for 30 s, repeated 24 times; (3) 72 °C for 5 min; and (4) held at 10 °C.

Fungal ITS2 DNA was amplified using 2.5 µl DNA template, 12.5 µl KAPA HiFi HotStart ReadyMix, 2 µM primers fITS7 (5′- TCGTCGGCAGCGTCAGATGTGTATAAGAGACAGGTGARTCATCGAATCTTTG-3′) and ITS4-Rev (5′-GTCTCGTGGGCTCGGAGATGTGTATAAGAGACAGTCCTCCGCTTATTGATATGC-3′) with Illumina adaptor sequences in combination with 2 µM blocking primers cl1ITS2-F (5′-CGTCTGCCTGGGTGTCACAAATCGTCGTCC-3′) and clITS2-R (5′- CCTGGTGTCGCTATATGGACTTTGGGTCAT-3′) in 25 µl reactions[43]. Cycling conditions for ITS2 were (1) 95 °C for 3 min; (2) 95 °C for 30 s, 55 °C for 30 s and 72 °C for 30 s, repeated 9 times; (3) 72 °C for 5 min; and (4) held at 10 °C.

For both PCR reactions, DNA was cleaned using the KingFisher Flex Purification System. Vortexed AMPure XP Beads (20 µl; Beckman Coulter) were added to 25 µl of PCR product in a KingFisher 96 deep-well plate. Beads with adjoined DNA were washed by subsequent transfer to 3 KingFisher 96 deep-well plates with 80% ethanol and DNA was then eluted in 30 µl C6 elution buffer from the Qiagen Powersoil KF kit.

Index PCR reactions were performed using standard Illumina i7 index primers (N701–N712) for columns and Illumina i5 index primers (N501–N508) for rows of each plate. DNA sample (5 µl) was added to a mix of 2.5 µl 2 µM index primer, 12.5 µl KAPA HiFi HotStart ReadyMix and 5 µl Milli-Q H_2O. Cycling conditions for index PCRs were (1) 95 °C for 3 min; (2) 95 °C for 30 s, 55 °C for 30 s and 72 °C for 30 s, repeated 9 times for 16S or 24 times for ITS2; (3) 72 °C for 5 min; and (4) held at 10 °C. After the index PCR, DNA was cleaned using the above-mentioned cleaning protocol. DNA concentrations of all PCR products were measured using a Qubit Flex Fluorometer with the Qubit dsDNA BR Assay Kit (Invitrogen) and normalized to 2 ng μl^{-1}, after which the samples were pooled and sent for Illumina V3 2×300 bp MiSeq sequencing at USEQ. Step-by-step protocols for DNA isolation and library preparations are available at ref. 56.

Microbial community analysis

Both 16S and ITS2 ribosomal DNA raw sequencing reads were denoised, joined, delineated into ASVs and assigned taxonomy in the Qiime2 (v.2019.7) environment[57]. Datasets were demultiplexed and then filtered using the DADA2 pipeline[58]. ASVs with less than 30 reads or present in less than 2 samples across all samples within a dataset were removed to minimize potential errors in sequencing. The representative sequences were subsequently taxonomically classified using a classifier trained with the 99% operational taxonomic unit threshold SILVA database[59] for bacteria and UNITE reference database (v.8.0) for fungi[60]. For bacteria, we removed the remaining 16S reads annotated as mitochondria or chloroplasts and kept only reads assigned to Bacteria. In addition, we removed a single ASV (258888d59976d9f8e12b0e5bb78be7ee) that was abundantly present in blank controls and was considered a contamination. We omitted ASVs identified as *Salinibacter ruber*, which was added externally as a standard (https://en.wikipedia.org/wiki/Salinibacter_ruber). For fungi, we removed the remaining ITS reads assigned as Viridiplantae and Protista and kept only reads assigned to Fungi. The datasets from seed tuber samples were rarefied to 8,000 bacterial and 4,000 fungal reads per sample. Bray–Curtis dissimilarity matrices were created in QIIME2 and visualized in R (v.4.0.3) using the Qiime2R (v.0.99.6) and ggplot2 package (v.3.4.4). Permutational multivariate analysis of variance (999 permutations) tests were performed using QIIME2 to test the effect of different factors on the microbiome composition.

Modelling and statistics

RF regression models were built on various taxonomy ranks including ASV, species, genus, family, order, class, phylum and features generated by HFE[28] using the randomForest package (v.4.6.14) in R with default parameters[27,61]. Models were developed independently for both eye or heel-end compartment using bacterial, fungal, and a combination of both bacterial and fungal datasets. Models on all phylogenetic levels are built with 1,000 trees with unrestricted growth. To assess the OOB error, the predicted values of the input data were generated using OOB samples. This method involves using data points that were not included in the bootstrap sample used to train a particular model.

We trained the models on the microbiome samples of year 2 and CSA in trial field M in the same year (training set). We tested the model by correlating the predicted CSA to the observed CSA in the two other trial fields of the same year (within-year testing set). We then tested the RF model further with the tuber microbiomes from year 1 (across-year testing set) originating from a completely distinct collection of seedlots.

The seedlots were divided into three classes of high (H), medium (M) and low (L) vigour by determining the three classes of the predicted and observed vigour. The three classes are values that divide a sample vector into three portions of equal probability; in our case, when the probability distribution of vigour is unknown, these are values that divide a given vector into portions of the same size. Samples have low vigour if their measured or predicted vigour measure is smaller than the first class, medium if it is between the first and second class and high if it is greater than the second class.

To measure the performance of the classification model, we compute the class-specific precision measure for a class C_i as:

$$\text{Precision}\,(C_i) = \frac{\text{True positives}\,(C_i)}{\text{True positives}\,(C_i) + \text{False positives}\,(C_i)}$$

that is, the ratio of correctly classified samples in C_i over the total number of samples

classified as C_i. Note that in terms of conditional probabilities for a seedlot x, this is equivalent to:

$$P(C_i|C_i) = \mathbb{P}(x\ \text{measured}\ C_i|x\ \text{predicted}\ C_i) = \frac{\mathbb{P}(x\ \text{predicted}\ C_i \cap x\ \text{measured}\ C_i)}{\mathbb{P}(x\ \text{predicted}\ C_i)}$$

Intuitively, a good classification model will have values close to one on the diagonal and low values off diagonal, indicating that the probability of a sample to be misclassified is much lower than the probability of being classified correctly. We define the quality confidence of the prediction as one minus the probability of the sample being misclassified as the opposite extremum. Whether the quality confidence is significantly higher than random chance was indicated by pseudo-P generated through 1,000 simulations of random classification.

Identification of keystone microorganisms

The importance of each ASV was extracted from the model using the importance() function in the randomForest package[27]. Briefly, this importance metric represents the change in the error of the model after permuting the counts of each of the ASVs and is therefore a measure of the contribution of each separate ASV to the model. This change is

calculated for different permutations of the OOB data, averaged across trees and normalized by the standard deviation of all values. The top 1% and 5% of these values were used to obtain the most strongly contributing ASVs. Partial dependence is defined as the individual effect of each ASV to the model prediction and was calculated using the hstats package[62] in R for the top 1% most-contributing ASVs.

Statistics and reproducibility

Tuber seedlots of 6 varieties from 180 fields per year were planted in each of 3 trial fields. In each of the three trial fields, the seed tubers were planted in a randomized block design with four replicate blocks. All microbiome samples were randomized during DNA isolation and amplicon sequencing. We applied Spearman's rank correlation in this study, which doesn't assume normality or any specific distribution of the data.

Reporting summary

Further information on research design is available in the Nature Portfolio Reporting Summary linked to this article.

Data availability

The raw sequence data generated from this study are available at https://www.ncbi.nlm.nih.gov/bioproject/PRJNA1091851/. Raw and spatial-corrected vigour data generated in this project and step-by-step protocol are available at https://data.4tu.nl/datasets/21892a06-078a-4600-8386-1abe46f42271. Source data are provided with this paper.

Code availability

The data and code used for modelling can be accessed through the following GitHub link: https://github.com/Yang-kf/Seed-tuber-microbiome-is-a-predictor-of-next-season-potato-vigor/tree/main.

References

1. Hiltner, L. Über neuere Erfahrungen und Probleme auf dem Gebiet der Bodenbakteriologie und unter besonderer Berücksichtigung der Gründüngung und Brache. *Arb. Dtsch. Landwirtsch. Ges.* **98**, 59–78 (1904).
2. Berendsen, R. L., Pieterse, C. M. J. & Bakker, P. A. H. M. The rhizosphere microbiome and plant health. *Trends Plant Sci.* **17**, 478–486 (2012).
3. Rolfe, S. A., Griffiths, J. & Ton, J. Crying out for help with root exudates: adaptive mechanisms by which stressed plants assemble health-promoting soil microbiomes. *Curr. Opin. Microbiol.* **49**, 73–82 (2019).
4. Teixeira, P. J. P., Colaianni, N. R., Fitzpatrick, C. R. & Dangl, J. L. Beyond pathogens: microbiota interactions with the plant immune system. *Curr. Opin. Microbiol.* **49**, 7–17 (2019).
5. Haney, C. H., Samuel, B. S., Bush, J. & Ausubel, F. M. Associations with rhizosphere bacteria can confer an adaptive advantage to plants. *Nat. Plants* **1**, 15051 (2015).
6. Goossens, P. et al. Obligate biotroph downy mildew consistently induces near-identical protective microbiomes in *Arabidopsis thaliana*. *Nat. Microbiol.* **8**, 2349–2364 (2023).
7. Raaijmakers, J. M., Paulitz, T. C., Steinberg, C., Alabouvette, C. & Moënne-Loccoz, Y. The rhizosphere: a playground and battlefield for soilborne pathogens and beneficial microorganisms. *Plant Soil* **321**, 341–361 (2009).
8. Thomas, G. & Sansonetti, G. *New Light on a Hidden Treasure: International Year of the Potato 2008, an End-of-Year Review* (Food and Agriculture Organization of the United Nations, 2009).
9. Devaux, A., Kromann, P. & Ortiz, O. Potatoes for sustainable global food security. *Potato Res.* **57**, 185–199 (2014).
10. Zarzyńska, K., Boguszewska-Mańkowska, D., Feledyn-Szewczyk, B. & Jończyk, K. The vigor of seed potatoes from organic and conventional systems. *Agriculture* **12**, 1764 (2022).
11. Struik, P. C. The canon of potato science: 40. physiological age of seed tubers. *Potato Res.* **50**, 375–377 (2007).
12. Zou, C. et al. Using sprouting behaviour to quantify physiological ageing of seed tubers of potato (*Solanum tuberosum* L.). *Environ. Exp. Bot.* **219**, 105648 (2024).
13. Bak, G.-R. et al. The potato rhizosphere microbiota correlated to the yield of three different regions in Korea. *Sci. Rep.* **14**, 4536 (2024).
14. Song, Y. et al. Seed tuber imprinting shapes the next-generation potato microbiome. *Environ. Microbiome* **19**, 12 (2024).
15. Kurm, V., Mendes, O., Gros, J. & van der Wolf, J. Potato tuber origin and microbial composition determines resistance against soft rot Pectobacteriaceae. *Eur. J. Plant Pathol.* **168**, 383–399 (2024).
16. Shi, W. et al. The occurrence of potato common scab correlates with the community composition and function of the geocaulosphere soil microbiome. *Microbiome* **7**, 14 (2019).
17. Arseneault, T., Goyer, C. & Filion, M. Biocontrol of potato common scab is associated with high *Pseudomonas fluorescens* LBUM223 populations and phenazine-1-carboxylic acid biosynthetic transcript accumulation in the potato geocaulosphere. *Phytopathology* **106**, 963–970 (2016).
18. Petrushin, I. S., Filinova, N. V. & Gutnik, D. I. Potato microbiome: relationship with environmental factors and approaches for microbiome modulation. *Int. J. Mol. Sci.* **25**, 750 (2024).
19. Fiers, M. et al. Potato soil-borne diseases. A review. *Agron. Sustain. Dev.* **32**, 93–132 (2012).
20. Van der Wolf, J. M. & De Boer, S. H. in *Potato Biology and Biotechnology* (eds. Vreugdenhil, D. et al.) 595–617 (Elsevier Science, 2007).
21. Bakker, P. A. H. M., Bakker, A. W., Marugg, J. D., Weisbeek, P. J. & Schippers, B. Bioassay for studying the role of siderophores in potato growth stimulation by *Pseudomonas spp* in short potato rotations. *Soil Biol. Biochem.* **19**, 443–449 (1987).
22. Buchholz, F., Antonielli, L., Kostić, T., Sessitsch, A. & Mitter, B. The bacterial community in potato is recruited from soil and partly inherited across generations. *PLoS ONE* **14**, e0223691 (2019).
23. Delventhal, K., Busby, P. E. & Frost, K. Tare soil alters the composition of the developing potato rhizosphere microbiome. *Phytobiomes J.* **7**, 91–99 (2023).
24. Deng, Z., Zhang, J., Li, J. & Zhang, X. Application of deep learning in plant-microbiota association analysis. *Front. Genet.* **12**, 697090 (2021).
25. Emmenegger, B. et al. Identifying microbiota community patterns important for plant protection using synthetic communities and machine learning. *Nat. Commun.* **14**, 7983 (2023).
26. Yuan, J. et al. Predicting disease occurrence with high accuracy based on soil macroecological patterns of Fusarium wilt. *ISME J.* **14**, 2936–2950 (2020).
27. Breiman, L. Random forests. *Mach. Learn.* **45**, 5–32 (2001).
28. Oudah, M. & Henschel, A. Taxonomy-aware feature engineering for microbiome classification. *BMC Bioinf.* **19**, 227 (2018).
29. Atza, E. & Budko, N. High-throughput analysis of potato vitality. In *Progress in Industrial Mathematics at ECMI 2021* (eds Ehrhardt, M. & Günther, M.) 273–279 (Springer, 2022).
30. Lottmann, J., Heuer, H., Smalla, K. & Berg, G. Beneficial bacteria in underground organs of potato (*Solanum tuberosum* L.). In *Proc. 7th International Verticillium Congress* (eds Tjamos, E. C. et al.) 264–268 (1997).
31. Clulow, S. A., Stewart, H. E., Dashwood, E. P. & Wastie, R. L. Tuber surface microorganisms influence the susceptibility of potato tubers to late blight. *Ann. Appl. Biol.* **126**, 33–43 (1995).
32. Aliche, E. B. et al. Drought response in field grown potatoes and the interactions between canopy growth and yield. *Agric. Water Manag.* **206**, 20–30 (2018).
33. Zhou, Z., Plauborg, F., Parsons, D. & Andersen, M. N. Potato canopy growth, yield and soil water dynamics under different irrigation systems. *Agric. Water Manag.* **202**, 9–18 (2018).

34. Haverkort, A. J. & Bicamumpaka, M. Correlation between intercepted radiation and yield of potato crops infested by *Phytophthora infestans* in central Africa. *Neth. J. Plant Pathol.* **92**, 239–247 (1986).
35. de Jesus Colwell, F. et al. Development and validation of methodology for estimating potato canopy structure for field crop phenotyping and improved breeding. *Front. Plant Sci.* **12**, 612843 (2021).
36. Rasche, F. et al. Impact of transgenic potatoes expressing anti-bacterial agents on bacterial endophytes is comparable with the effects of plant genotype, soil type and pathogen infection. *J. Appl. Ecol.* **43**, 555–566 (2006).
37. Manter, D. K., Delgado, J. A., Holm, D. G. & Stong, R. A. Pyrosequencing reveals a highly diverse and cultivar-specific bacterial endophyte community in potato roots. *Microb. Ecol.* **60**, 157–166 (2010).
38. Fierer, N. Embracing the unknown: disentangling the complexities of the soil microbiome. *Nat. Rev. Microbiol.* **15**, 579–590 (2017).
39. Benitez, M.-S., Osborne, S. L. & Lehman, R. M. Previous crop and rotation history effects on maize seedling health and associated rhizosphere microbiome. *Sci. Rep.* **7**, 15709 (2017).
40. Hartmann, M., Frey, B., Mayer, J., Mäder, P. & Widmer, F. Distinct soil microbial diversity under long-term organic and conventional farming. *ISME J.* **9**, 1177–1194 (2015).
41. Lutz, S. et al. Soil microbiome indicators can predict crop growth response to large-scale inoculation with arbuscular mycorrhizal fungi. *Nat. Microbiol.* **8**, 2277–2289 (2023).
42. Zuno-Floriano, F. G. et al. Effect of *Acinetobacter* sp. on metalaxyl degradation and metabolite profile of potato seedlings (*Solanum tuberosum L.*) alpha variety. *PLoS ONE* **7**, e31221 (2012).
43. Schlatter, D., Kinkel, L., Thomashow, L., Weller, D. & Paulitz, T. Disease suppressive soils: new insights from the soil microbiome. *Phytopathology* **107**, 1284–1297 (2017).
44. Bowers, J. H., Kinkel, L. L. & Jones, R. K. Influence of disease-suppressive strains of *Streptomyces* on the native *Streptomyces* community in soil as determined by the analysis of cellular fatty acids. *Can. J. Microbiol.* **42**, 27–37 (1996).
45. Liu, D., Anderson, N. A. & Kinkel, L. L. Biological control of potato scab in the field with antagonistic *Streptomyces scabies*. *Phytopathology* **85**, 827–831 (1995).
46. Wanner, L. A. High proportions of nonpathogenic *Streptomyces* are associated with common scab-resistant potato lines and less severe disease. *Can. J. Microbiol.* **53**, 1062–1075 (2007).
47. Friedman, J. H. Greedy function approximation: a gradient boosting machine. *Ann. Stat.* **29**, 1189–1232 (2001).
48. Hernández Medina, R. et al. Machine learning and deep learning applications in microbiome research. *ISME Commun.* **2**, 98 (2022).
49. Pasolli, E., Truong, D. T., Malik, F., Waldron, L. & Segata, N. Machine learning meta-analysis of large metagenomic datasets: tools and biological insights. *PLoS Comput. Biol.* **12**, e1004977 (2016).
50. Ditzler, G., Morrison, J. C., Lan, Y. & Rosen, G. L. Fizzy: feature subset selection for metagenomics. *BMC Bioinform.* **16**, 358 (2015).
51. Zhou, Y. & Gallins, P. A review and tutorial of machine learning methods for microbiome host trait prediction. *Front. Genet.* **10**, 579 (2019).
52. Jones, J. D. & Dangl, J. L. The plant immune system. *Nature* **444**, 323–329 (2006).
53. Wintermans, P. C. A., Bakker, P. A. H. M. & Pieterse, C. M. J. Natural genetic variation in *Arabidopsis* for responsiveness to plant growth-promoting rhizobacteria. *Plant Mol. Biol.* **90**, 623–634 (2016).
54. Rodríguez-Álvarez, M. X., Boer, M. P., van Eeuwijk, F. A. & Eilers, P. H. C. Correcting for spatial heterogeneity in plant breeding experiments with P-splines. *Spat. Stat.* **23**, 52–71 (2018).
55. Atza, E. & Budko, N. Data underlying the publication: Seed tuber microbiome is a predictor of next-season potato vigor. *4TU. ResearchData* https://doi.org/10.4121/21892a06-078a-4600-8386-1abe46f42271 (2024).
56. Song, Y., Jongekrijg, C. D., Manders, E. J. H. H. & de Rooil, P. Flight-to-vitality project microbiome sequencing protocols. *Zenodo* https://doi.org/10.5281/zenodo.10955437 (2024).
57. Bolyen, E. et al. Reproducible, interactive, scalable and extensible microbiome data science using QIIME 2. *Nat. Biotechnol.* **37**, 852–857 (2019).
58. Callahan, B. J. et al. DADA2: high-resolution sample inference from Illumina amplicon data. *Nat. Methods* **13**, 581–583 (2016).
59. Quast, C. et al. The SILVA ribosomal RNA gene database project: improved data processing and web-based tools. *Nucleic Acids Res.* **41**, 590–596 (2013).
60. Abarenkov, K. et al. The UNITE database for molecular identification of fungi–recent updates and future perspectives. *N. Phytol.* **186**, 281–285 (2010).
61. Breiman, L. *Manual on Setting Up, Using, and Understanding Random Forests v3.1* (Statistics Department Univ. California Berkeley, 2002).
62. Friedman, J. H. & Popescu, B. E. Predictive learning via rule ensembles. *Ann. Appl Stat.* **2**, 916–954 (2008).

Acknowledgements

We acknowledge the valuable contributions of the Royal HZPC Group B.V. and Averis Seeds B.V. for providing the seed tuber material and supporting the field trials. Their collaboration was essential to the successful execution of this research. Special thanks are extended to F. Hofstra and M. ten Klooster from HZPC Holding B.V. for their contribution to the sample collection and J. Hopman from Averis Seeds B.V. for his valuable advice. We also thank C. Jongekrijg, E. Manders and E. de Kloe for excellent technical assistance in the laboratory. In addition, we acknowledge the funding support received from Europees Landbouwfonds voor Plattelandsontwikkeling (ELFPO) on the 'Flight-to-vitality' project. This work was also partly supported by the Dutch Research Council (NWO) through the Gravitation program MiCRop (grant number 024.004.014) and through project 'Sequence-based POTato Microbiome tools for microbiome-optimized potatoes' (project number 19769).

Author contributions

Y.S., D.A., E.A., N.V.B., R.d.J., P.A.H.M.B., C.M.J.P. and R.L.B. designed the experiments and approach. Y.S., E.A., J.J.S.G., N.V.B., P.A.H.M.B., C.M.J.P. and R.L.B. wrote the article. D.A. coordinated sampling collection and experimental field trials. Y.S. and P.G.H.d.R. carried out molecular analysis. E.A. and N.V.B. performed quantitative analysis of drone images and CSA data. Y.S., E.A., J.J.S.G., R.d.J. and D.K. performed data analysis.

Competing interests

The authors declare that this study received funding from HZPC Research B.V. and Averis Seeds B.V. The funder had the following involvement in the study: study design, sample collection and the decision to submit it for publication. D.A. is a current employee of HZPC Research B.V. All other authors declare no competing interests.

Additional information

Extended data is available for this paper at https://doi.org/10.1038/s41564-024-01872-x.

Supplementary information The online version contains supplementary material available at https://doi.org/10.1038/s41564-024-01872-x.

Correspondence and requests for materials should be addressed to Roeland L. Berendsen.

Peer review information *Nature Microbiology* thanks Yang Bai, Alireza Pourreza, Detlef Weigel and the other, anonymous, reviewer(s) for their contribution to the peer review of this work. Peer reviewer reports are available.

[1]Plant–Microbe Interactions, Institute of Environmental Biology, Department of Biology, Science4Life, Utrecht University, Utrecht, the Netherlands. [2]Numerical Analysis, Delft Institute of Applied Mathematics, Faculty of Electrical Engineering, Mathematics and Computer Science, Delft University of Technology, Delft, the Netherlands. [3]HZPC Research B.V., Department of Plant Pathology, Metslawier, the Netherlands. [4]AI Technology for Life, Department of Information and Computing Sciences, Science4Life, Utrecht University, Utrecht, the Netherlands. ✉e-mail: r.l.berendsen@uu.nl

https://doi.org/10.1038/s41564-024-01872-x

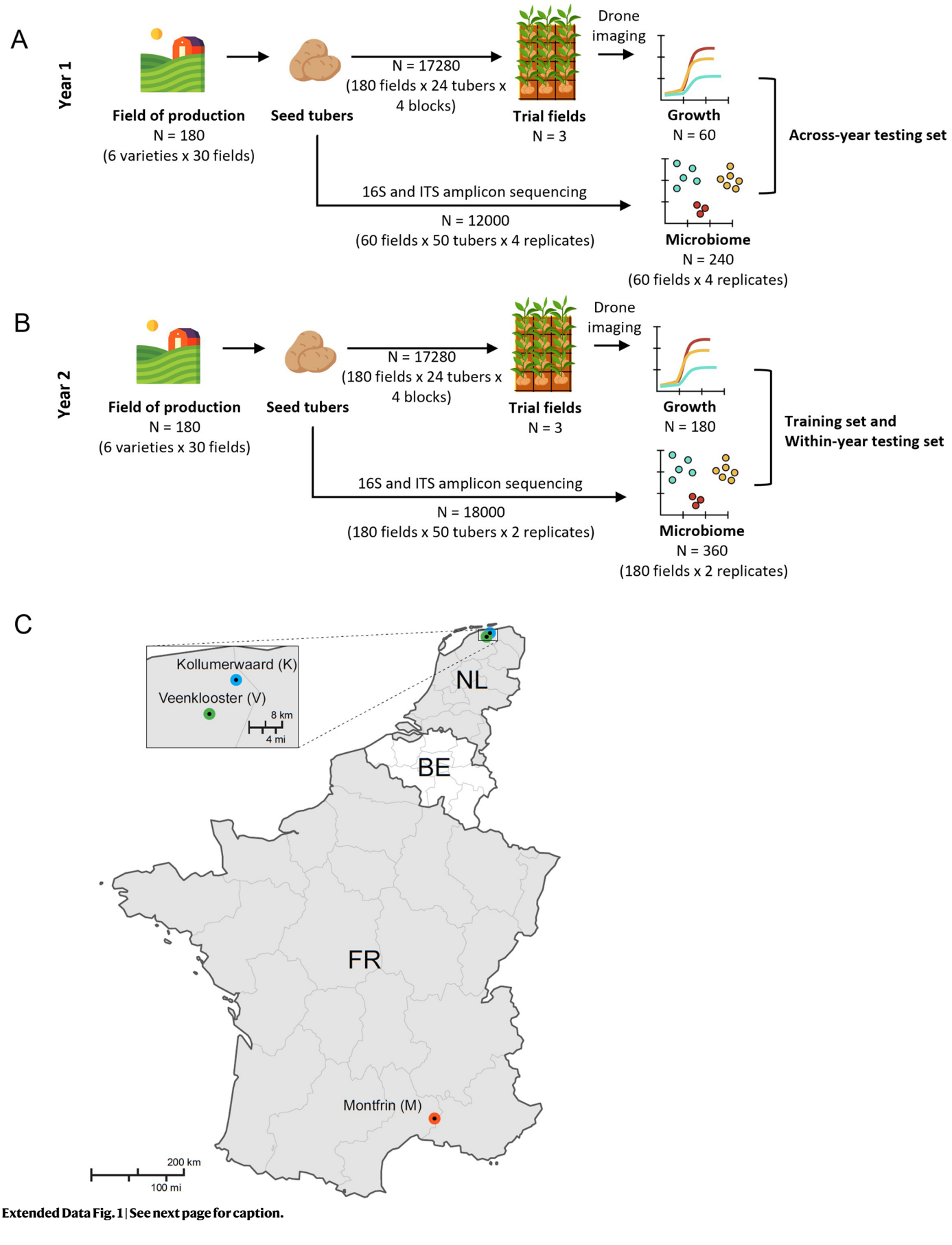

Extended Data Fig. 1 | See next page for caption.

https://doi.org/10.1038/s41564-024-01872-x

Extended Data Fig. 1 | Experimental design for over 2 years. a-b We collected seed tubers of 6 potato varieties from 30 fields per variety (180 fields in total) in the Netherlands in the autumn of 2018 (year 1) and 2019 (year 2). Tubers from these 180 fields per year were stored over winter and the tubers were planted in each of 3 trial fields in the next spring. **c** In both years, the trial fields were located near Montfrin (M) in France and near Kollumerwaard (K) and Veenklooster (V) in the Netherlands. In each of the trial fields, the seed tubers were planted in randomized block design with 4 replicate blocks of 24 tubers. We monitored the growth and development of the plants that emerged from these seed tubers using aerial images of the complete field with a drone-mounted camera. Of the 180 seedlots of year 1, we selected 60 seedlots from which we took 4 replicate samples for microbiome analysis. In year 2, the microbiomes were analyzed with 2 replicate samples of all 180 seedlots. Credit: icons in **a**,**b**, Flaticon.com.

https://doi.org/10.1038/s41564-024-01872-x

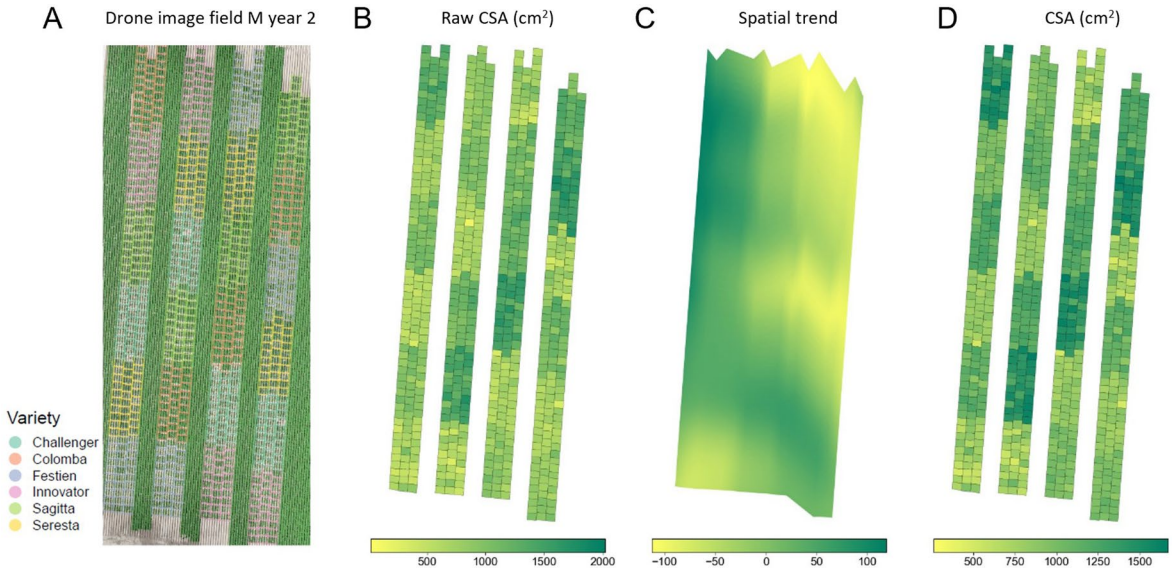

Extended Data Fig. 2 | From field images to potato vigor data. a Exemplary ortho image of trial field M in year 2 obtained with drone-mounted camera. Plot boundaries of each seedlot are displayed in variety-specific colors. **b** Overview of raw canopy surface area (raw CSA) per plot in the trial field displayed as a heatmap. **c** Spatial trend of the trial field recovered with the SpaTS package and displayed as a heatmap. **d** Overview of spatially corrected raw CSA in the trial field as a heatmap. Average corrected seedlot CSA is shown in all replicate plots of the four seedlots.

https://doi.org/10.1038/s41564-024-01872-x

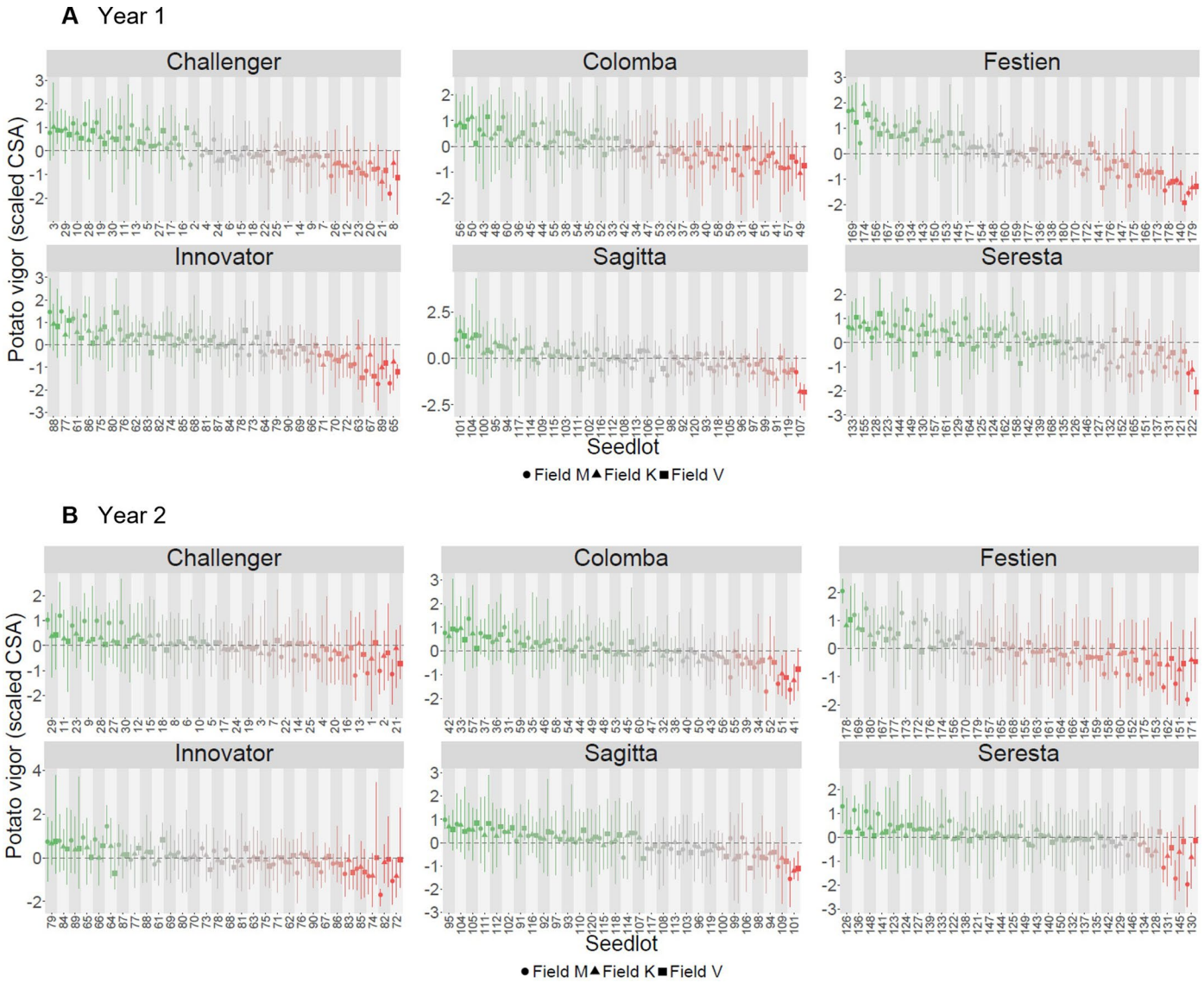

Extended Data Fig. 3 | Potato vigour of a seedlot is consistent across three trial fields. a Scaled CSA for each of the 6 varieties and each of the 30 seedlots per variety in Field M, K and V in year 1. **b** Scaled CSA for each of the 6 varieties and each of the 30 seedlots per variety in Field M, K and V in year 2. Error bars signify the minimum and maximum values for a given seed lot per trial field. The CSA in each trial field, as estimated by the SpaTS package, is indicated with the field corresponding marker (see legend).

https://doi.org/10.1038/s41564-024-01872-x

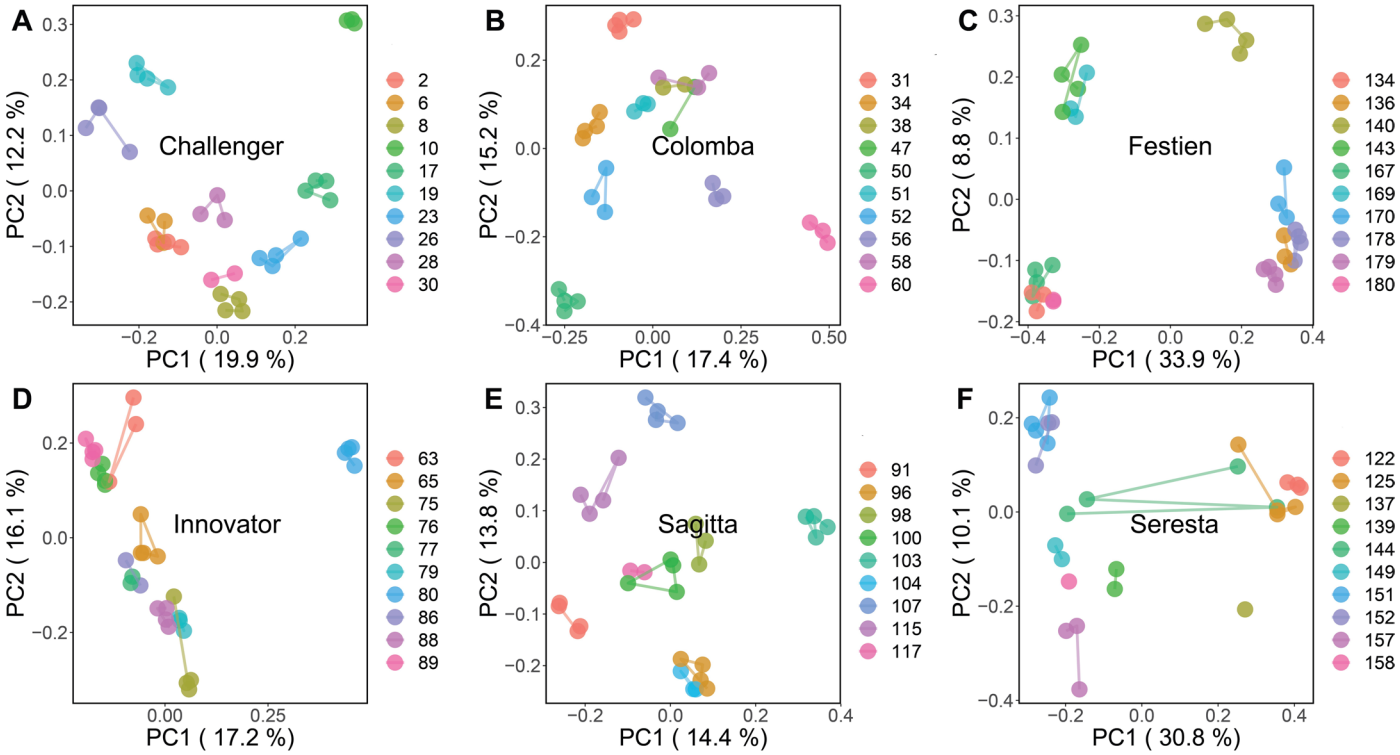

Extended Data Fig. 4 | Microbiomes of replicate samples of the same seedlot cluster together in year 1. PCoA ordination plot based on Bray-Curtis dissimilarities of bacterial communities of seed tuber eye compartment from year 1. Variety names are indicated in each panel with Challenger (**a**), Colomba (**b**), Festien (**c**), Innovator (**d**), Sagitta (**e**) and Seresta (**f**). Each data point represents a replication of one seedlot. Different colors represent different seedlots of a variety.

https://doi.org/10.1038/s41564-024-01872-x

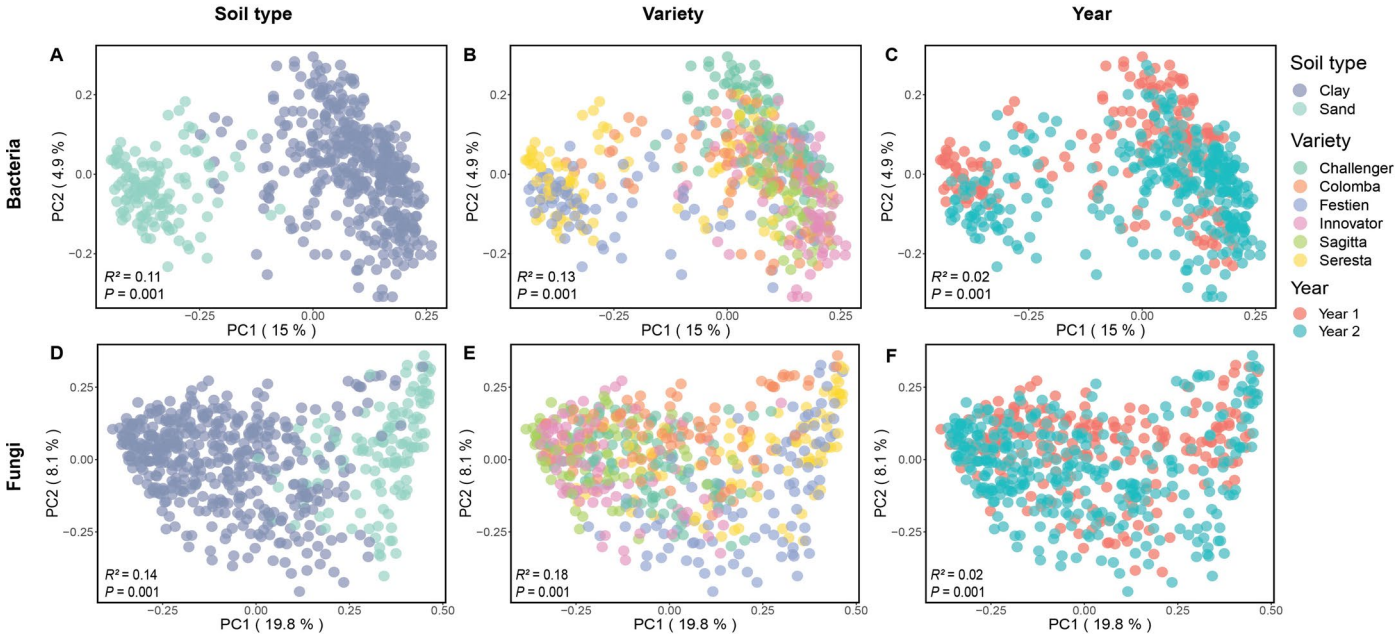

Extended Data Fig. 5 | Seed tuber microbiomes in heel end compartments. Principle coordinate analysis (PCoA) ordination plot based on Bray-Curtis dissimilarities of bacterial (**a-c**) and fungal (**d-f**) microbiomes. Symbols are colored by soil type (**a,d**), variety (**b,e**) and year (**c,f**) as indicated in the legend. Each data point represents a single replicate of a seedlot. Four replicate samples were analyzed for each of 60 seedlots in year 1 and two replicate samples for each of 180 seedlots in year 2. *P* (one-sided) and R^2 in each PCoA are the result of PERMANOVA on soil type (**a,d**), variety (**b,e**) and year (**c,f**) as respective factors.

https://doi.org/10.1038/s41564-024-01872-x

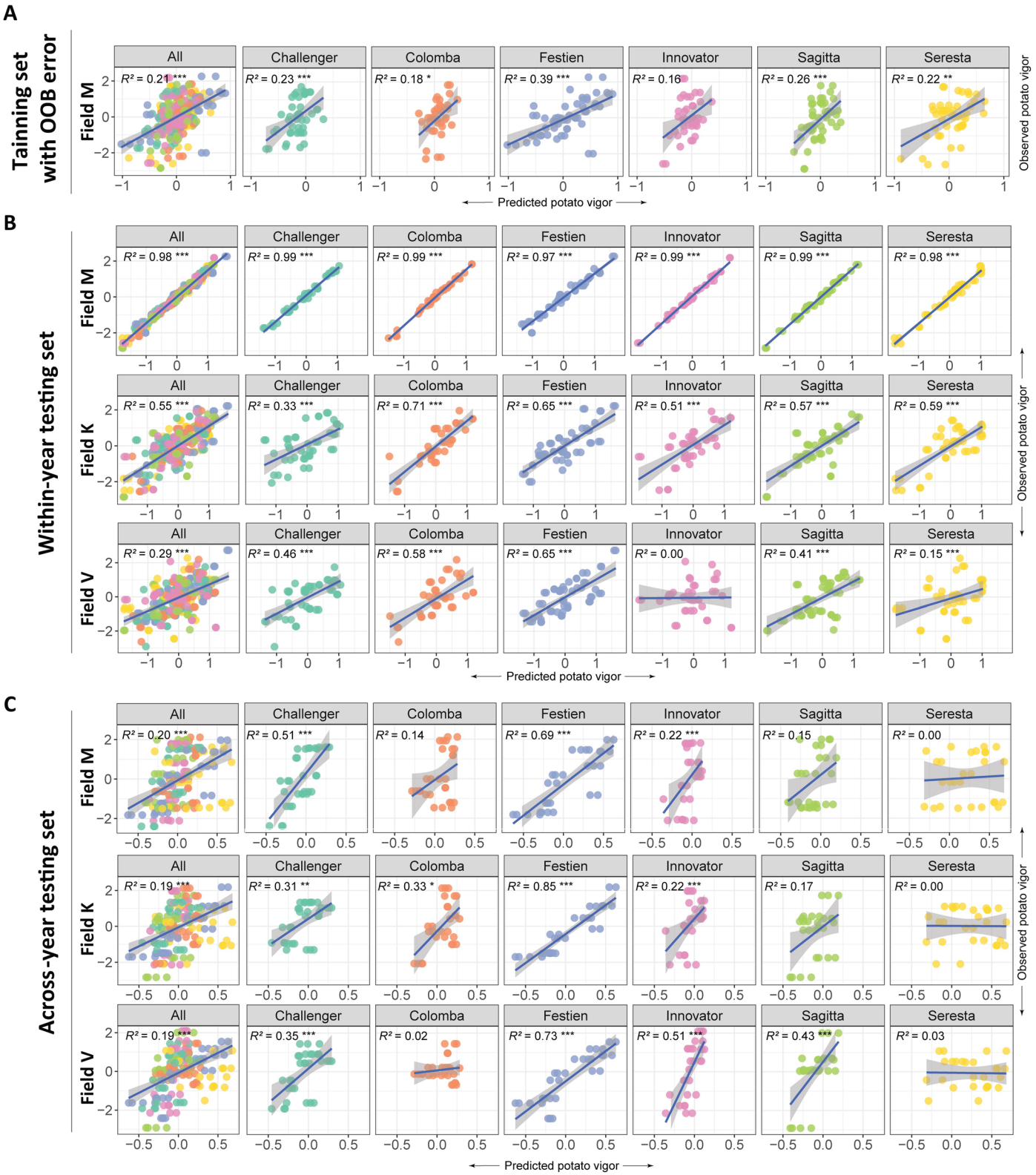

Extended Data Fig. 6 | Scatter plots illustrating the Pearson correlation between the predicted and observed potato vigor in all fields and varieties. **a**, Out-of-bag (OOB) model performance per variety. **b**, Model performance per variety on within-year test sets. **c**, Model performance per variety on across-year test sets. In all panels, values on the x-axis are predicted by a random forest model trained on microbiome data from year 2 and CSA from field M. The predicted potato vigor is based on the same microbiome data as was used for training the model (within-year testing set) or based on microbiome data from year 1 to which the model was naïve (across-year testing set). The 6 varieties are represented by different colors. Each symbol represents a prediction microbiome based on 1 eye compartment sample. Predicted and observed vigor are indicated by scaled CSA, which is scaled to the variety average in each trial field. The proportion of variance explained by the model is indicated by R^2. Asterisks indicate significance level of $^*P < 0.05$; $^{**}P < 0.01$; $^{***}P < 0.001$; $^{****}P < 0.0001$, two-sided. Error bands around the regression line represent 95% confidence interval.

https://doi.org/10.1038/s41564-024-01872-x

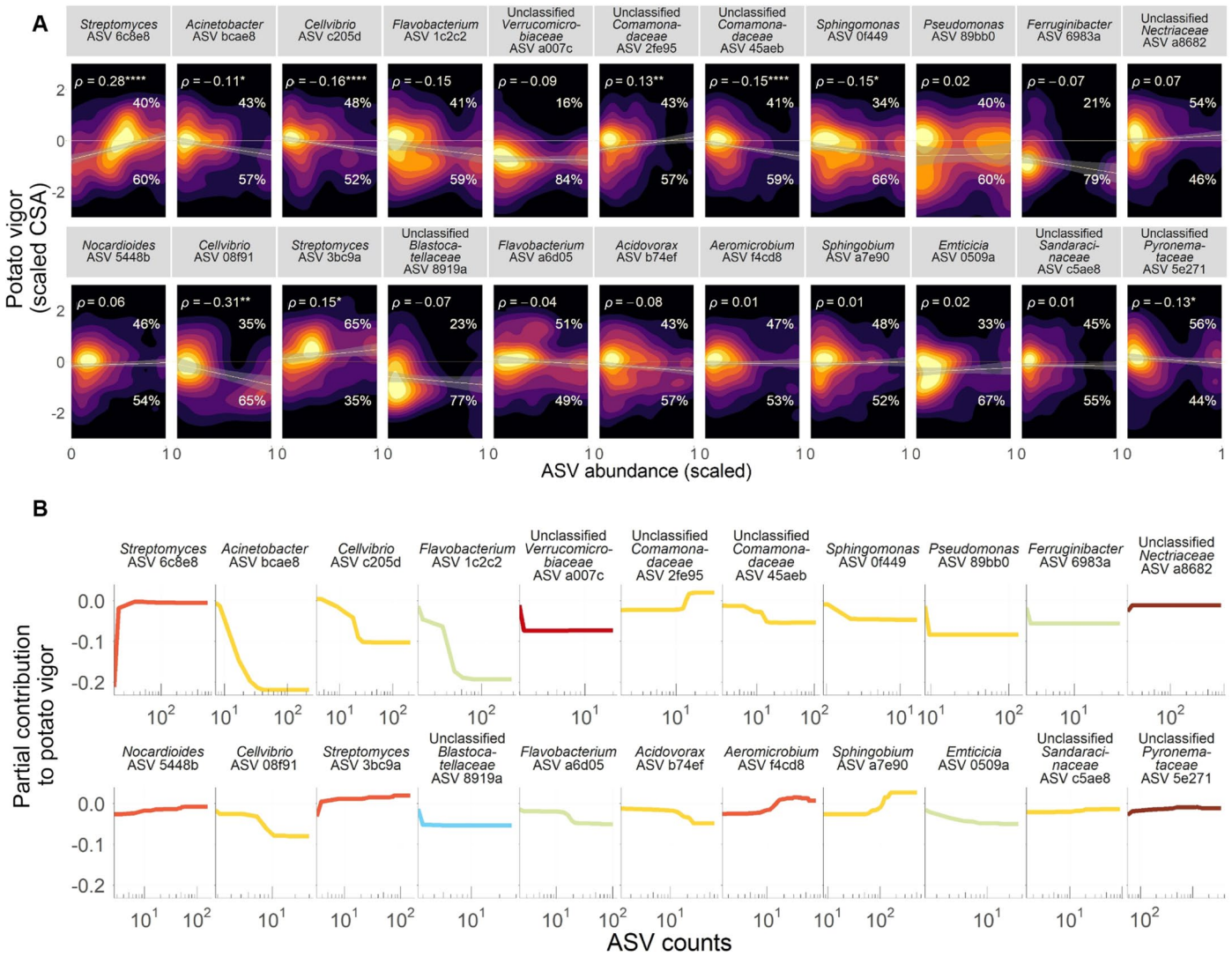

Extended Data Fig. 7 | General assessment of the relationship between the top 1% contributors to potato vigor. a Bidimensional density plots showing scaled CSA values and normalized abundance of each of the top 1% contributing ASVs. ASV abundance is rescaled between 0 and 1 with respect to their minimum and maximum in order to show one single scale across ASVs. The clearest colors indicate areas that accumulate most of the data, and dark colors the areas where no data or few points are found. The line was fitted with a robust regression to outliers computed with the *rlm()* functions in the *MASS* R package, and the ρ values indicate Spearman's ρ together with the significance level shown by asterisks (*$P < 0.05$; **$P < 0.01$; ***$P < 0.001$; ****$P < 0.0001$, two-sided). The percentages above and below the 0-line indicate the number of ASV occurrences in sample with vigor above and below the mean, respectively. **b** Partial contribution plots for the top 1% ASVs most predictive to potato vigor (scaled CSA) according to the RF model.

https://doi.org/10.1038/s41564-024-01872-x

Extended Data Fig. 8 | Heatmaps showing Spearman correlations of each of the top 1% contributing ASVs to potato vigor, their prevalence, and median abundance across samples. The first column in every heatmap shows the computed value including all the data regardless of plant variety, and the rest of columns display those values calculated for individual potato varieties. The abundance of the fungal ASVs were shown as 1/10 of the original value to fit in the color scale. The significance level of Spearman's ρ are shown by asterisks (*$P < 0.05$; **$P < 0.01$; ***$P < 0.001$; ****$P < 0.0001$).

nature portfolio

Corresponding author(s): Roeland Berendsen

Last updated by author(s): Oct 23, 2024

Reporting Summary

Nature Portfolio wishes to improve the reproducibility of the work that we publish. This form provides structure for consistency and transparency in reporting. For further information on Nature Portfolio policies, see our Editorial Policies and the Editorial Policy Checklist.

Statistics

For all statistical analyses, confirm that the following items are present in the figure legend, table legend, main text, or Methods section.

n/a	Confirmed	
☐	☒	The exact sample size (*n*) for each experimental group/condition, given as a discrete number and unit of measurement
☐	☒	A statement on whether measurements were taken from distinct samples or whether the same sample was measured repeatedly
☐	☒	The statistical test(s) used AND whether they are one- or two-sided *Only common tests should be described solely by name; describe more complex techniques in the Methods section.*
☐	☒	A description of all covariates tested
☐	☒	A description of any assumptions or corrections, such as tests of normality and adjustment for multiple comparisons
☐	☒	A full description of the statistical parameters including central tendency (e.g. means) or other basic estimates (e.g. regression coefficient) AND variation (e.g. standard deviation) or associated estimates of uncertainty (e.g. confidence intervals)
☐	☒	For null hypothesis testing, the test statistic (e.g. *F*, *t*, *r*) with confidence intervals, effect sizes, degrees of freedom and *P* value noted *Give P values as exact values whenever suitable.*
☒	☐	For Bayesian analysis, information on the choice of priors and Markov chain Monte Carlo settings
☐	☒	For hierarchical and complex designs, identification of the appropriate level for tests and full reporting of outcomes
☐	☒	Estimates of effect sizes (e.g. Cohen's *d*, Pearson's *r*), indicating how they were calculated

Our web collection on statistics for biologists contains articles on many of the points above.

Software and code

Policy information about availability of computer code

Data collection	No public data was used in this study.
Data analysis	Amplicon sequencing data was analysed in the Qiime2 environment (version 2019.7) or R (version 4.0.3) using packages as described on Online Methods section 'Microbial community analysis'. The representative sequences were taxonomically classified using athe SILVA database 59 for bacteria and UNITE reference database (v.8.0). Bray-Curtis dissimilarity matrices were created in QIIME2 and visualized in R (version 4.0.3) using the Qiime2R (v.0.99.6) and ggplot2 (v.3.4.4) package. Step-by-step protocols for DNA isolation and library preparations are available at https://doi.org/10.5281/zenodo.10955437. Field imaging data was processed with WebODM in year 1 and Agisoft in year 2 and analysed with an in-house standardized procedure, all of which is described in a step-by-step protocol: https://data.4tu.nl/datasets/21892a06-078a-4600-8386-1abe46f42271. Spatial effect removal was performed with the R-package SpATS (Version 1.0-19). Random forest regression models were built using the randomForest package (v.4.6.14) in R. Raw and spatial corrected vigor data generated in this project and step-by-step protocol can be found at https://data.4tu.nl/datasets/21892a06-078a-4600-8386-1abe46f42271. The data and code used for modeling can be accessed through the following GitHub link: https://github.com/Yang-kf/Seed-tuber-microbiome-is-a-predictor-of-next-season-potato-vigor/tree/main.

For manuscripts utilizing custom algorithms or software that are central to the research but not yet described in published literature, software must be made available to editors and reviewers. We strongly encourage code deposition in a community repository (e.g. GitHub). See the Nature Portfolio guidelines for submitting code & software for further information.

Data

Policy information about availability of data

All manuscripts must include a data availability statement. This statement should provide the following information, where applicable:

- Accession codes, unique identifiers, or web links for publicly available datasets
- A description of any restrictions on data availability
- For clinical datasets or third party data, please ensure that the statement adheres to our policy

Raw and spatial corrected vigor data generated in this project and step-by-step protocol can be found at https://data.4tu.nl/datasets/21892a06-078a-4600-8386-1abe46f42271. The raw sequence data generated of this study are available at https://www.ncbi.nlm.nih.gov/bioproject/PRJNA1091851/

Research involving human participants, their data, or biological material

Policy information about studies with human participants or human data. See also policy information about sex, gender (identity/presentation), and sexual orientation and race, ethnicity and racism.

Reporting on sex and gender	NA
Reporting on race, ethnicity, or other socially relevant groupings	NA
Population characteristics	NA
Recruitment	NA
Ethics oversight	NA

Note that full information on the approval of the study protocol must also be provided in the manuscript.

Field-specific reporting

Please select the one below that is the best fit for your research. If you are not sure, read the appropriate sections before making your selection.

☒ Life sciences ☐ Behavioural & social sciences ☐ Ecological, evolutionary & environmental sciences

For a reference copy of the document with all sections, see nature.com/documents/nr-reporting-summary-flat.pdf

Life sciences study design

All studies must disclose on these points even when the disclosure is negative.

Sample size	Cores from 50 seed tubers were pooled into a single sample per compartment per seedlot for each biological replicate. For each of the 6 varieties, we sampled 4 replicates for each of 10 seedlots in year 1 (240 samples per compartment) and 2 replicates of 30 seedlots in year 2 (360 samples per compartment). The sample sizes were maximized but limited by practical feasibility and available budget. In total, 30,000 tubers (12,000 in year 1 and 18,000 in year 2) were sampled to access the microbial composition of different tuber compartments, resulting in 600 samples per compartment. Preliminary analysis showed that replicate samples comprised very similar microbiomes, so for microbiome sequencing in year 2 we used only 2 replicate samples per seedlot.
Data exclusions	The datasets from seed tubers samples were rarefied to respectively 8000 bacterial and 4000 fungal reads per sample. Samples did not reach the minimal sequencing depth were excluded. Moreover, in the year 2 data we found a single amplicon sequence variant that had contaminated 2 sequencing runs and was also abundantly present in our blank control samples. We excluded this ASV from our data analysis.
Replication	This experiment was conducted in 3 different trail fields for 2 years. The trial fields were located in both years on farms near Montfrin (M, 54.4980 N, 5.1090 E) in France and near Kollumerwaard (K, 70.4325 N, 6.9825 E) and Veenklooster (V, 70.3935 N, 6.7080 E) in the north of the Netherlands, respectively.
Randomization	For vigor measurement: Tuber seedlots from 180 fields per year were planted in each of 3 trial fields in both years. In each of the trial fields, the seed tubers were planted in randomized block design with 4 replicate blocks of 24 tubers evenly distributed over 4 ridges. For microbiome profiling, all samples were randomized within each sequencing run and across 10 different runs.
Blinding	Not applicable, we only performed unbiased molecular analysis. This could not have been influenced by uncousious biases. It was not necessary to perform blinding. The high-throughput samples used in our study were randomized (described above).

Reporting for specific materials, systems and methods

We require information from authors about some types of materials, experimental systems and methods used in many studies. Here, indicate whether each material, system or method listed is relevant to your study. If you are not sure if a list item applies to your research, read the appropriate section before selecting a response.

Materials & experimental systems

n/a	Involved in the study
☒	☐ Antibodies
☒	☐ Eukaryotic cell lines
☒	☐ Palaeontology and archaeology
☒	☐ Animals and other organisms
☒	☐ Clinical data
☒	☐ Dual use research of concern
☐	☒ Plants

Methods

n/a	Involved in the study
☒	☐ ChIP-seq
☒	☐ Flow cytometry
☒	☐ MRI-based neuroimaging

Dual use research of concern

Policy information about dual use research of concern

Hazards

Could the accidental, deliberate or reckless misuse of agents or technologies generated in the work, or the application of information presented in the manuscript, pose a threat to:

No	Yes
☒	☐ Public health
☒	☐ National security
☒	☐ Crops and/or livestock
☒	☐ Ecosystems
☒	☐ Any other significant area

Experiments of concern

Does the work involve any of these experiments of concern:

No	Yes
☒	☐ Demonstrate how to render a vaccine ineffective
☒	☐ Confer resistance to therapeutically useful antibiotics or antiviral agents
☒	☐ Enhance the virulence of a pathogen or render a nonpathogen virulent
☒	☐ Increase transmissibility of a pathogen
☒	☐ Alter the host range of a pathogen
☒	☐ Enable evasion of diagnostic/detection modalities
☒	☐ Enable the weaponization of a biological agent or toxin
☒	☐ Any other potentially harmful combination of experiments and agents

Plants

Seed stocks	In total, 6 commercial potato varieties form the Royal HZPC Group and Averis Seeds B.V. were used in this study, namely variety Challenger (Variety A), Colomba (Variety B), Festien (Variety C), Innovator (Variety D), Sagitta (Variety E) and Seresta (Variety F).
Novel plant genotypes	NA
Authentication	NA